

Journal Pre-proofs

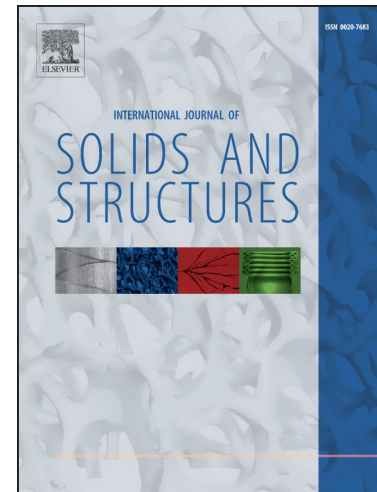
A linear-elastic heuristic-molecular modelling for plane isotropic micropolar and auxetic materials

Siro Casolo

PII: S0020-7683(21)00126-8
DOI: <https://doi.org/10.1016/j.ijsolstr.2021.111042>
Reference: SAS 111042

To appear in: *International Journal of Solids and Structures*

Received Date: 29 November 2020
Accepted Date: 23 March 2021



Please cite this article as: Casolo, S., A linear-elastic heuristic-molecular modelling for plane isotropic micropolar and auxetic materials, *International Journal of Solids and Structures* (2021), doi: <https://doi.org/10.1016/j.ijsolstr.2021.111042>

This is a PDF file of an article that has undergone enhancements after acceptance, such as the addition of a cover page and metadata, and formatting for readability, but it is not yet the definitive version of record. This version will undergo additional copyediting, typesetting and review before it is published in its final form, but we are providing this version to give early visibility of the article. Please note that, during the production process, errors may be discovered which could affect the content, and all legal disclaimers that apply to the journal pertain.

A linear-elastic heuristic-molecular modelling for plane isotropic micropolar and auxetic materials

Siro Casolo^{a,*}

^aDepartment ABC, Politecnico di Milano, Italy

Abstract

A discrete Lagrangian approach is the basis for modelling the macroscale elastic response of a solid material, which can be homogeneous as well as a periodic composite. The basic topology is a square “heuristic molecule” that is an assemblage of four rigid bodies with a definite shape bonded by elastic springs. This is the minimum unit cell, UC, that contains all the macroscopic mechanical properties of the solid material, object of study. The paper presents 4 unit cells, in progression from a basic molecule bonded by 2 types of central forces, to a refined “Cosserat-auxetic” molecule that is connected by 4 types of shear and central bond-springs. The emphasis is given to the isotropic response in relation to the value of the macroscopic Poisson ratio, and the four examples of UC topologies are presented showing their relationship to different materials at the macro-scale: from a “rari-constant” continuum, through a standard isotropic Cauchy continuum, up to an isotropic centre-symmetric auxetic Cosserat solid.

Keywords: elasticity, isotropy, Poisson’s ratio, heuristic molecule, rigid element, micro-structure, spring network model, Cosserat, auxetic, RBMS

1. Introduction

The macroscopic modelling of a solid material based on an intrinsically discrete approach is the frame in which the present research is inserted. It is well known how the continuum approach, originated by Green, predominates in the formulation of the elasticity problem, and this is a basis of the great success of the finite element method in the field of computational mechanics. Despite this, in modern mechanics, some full discrete approaches, or “structure theories” in the words of Love (1926), have also been proposed and supported. Interestingly, they have deep roots that date back to some first ideas proposed by Poisson (1831) along with Cauchy and Navier, up to the fundamental contribution of Voigt (1900) who overcame the “rari-constant” limitations of the early approaches (Foce, 1995; Capecchi et al., 2010). More

*Corresponding author, e-mail: siro.casolo@polimi.it

recently, the computational models based on structure theories, sometimes following a mechanistic approach, have attracted a renewed interest, especially for applications dealing with the post-failure behaviour of fragile and/or heterogeneous materials. In fact, modern materials and engineering constructions are often adopting composite materials with regular micro-structure for which the homogenized continuum description tends to become problematic when dealing with the concentration of deformations, and standard local models find some limits whenever the fracture process is addressed. Among the alternative approaches, the lattice models in which the solid is imagined as an assembly of masses connected by springs or a grid of beams, as well as the spring network models, or the numerical models based on peridynamics, are well established and increasingly appreciated by the scientific community (Bolander and Saito, 1998; Griffiths and Mustoe, 2001; Ostoja-Starzewski, 2002; Gerstle et al., 2007; Wang and Mora, 2008; Cusatis et al., 2011; Brighenti et al., 2013; Birck et al., 2016; Yao et al., 2016; Jiang et al., 2017; Ballarini et al., 2018; Diana and Carvelli, 2020; Eremeyev and Turco, 2020).

This manuscript outlines an heuristics in which the geometric and physical aspects are emphasized by adopting a mechanistic modelling based on an imaginary topology that perhaps can resound as an echo of the Donato Rossetti's ancient theory that matter is made of "atoms" that have "poles" which are the centres of fields of attractive or repulsive forces. In the seventeenth century, he called himself a "polist", and said: "if you do not take the poles of atoms and of molecules for granted, at least admit their existence as possible, and you will accordingly find all properties of bodies are demonstratively explained through them..." (Rossetti, 1671; Benvenuto, 1991).

Thence, the attention is here focused on the definition of a "unit cell" UC that should possess the essential characters to be perceived at the macro-scale. In this sense, the UC is also called "heuristic molecule" (Casolo, 2006), recalling the fact that it contains the essence of the solid material under consideration and it is the minimum element, below which the solid cannot be described. The atom here is just an abstract idea, so it should be clear that this is a philosophically "atomistic" approach, while the heuristic molecules are adopted as a mean to discretize the solid at the macro-scale, and a UC marks the minimum level of detail that can be described by the numerical model.

On the other hand, the computational structural mechanics requires to formulate the elasticity problems by means of a suitable process of discretization which does not always need the passage through a continuum medium description, and thus by means of a mathematical limit that restricts the physical solid structure to be an assemblage of "material points". A direct full discrete approach can be pursued then, without homogenization, by avoiding the passage through the continuum field (Tonti, 2001, 2014; Ferretti, 2013).

The program is to model the solid at the macroscale in computational terms basing the constitutive problem on a heuristic topology for the material, with the methodological attitude to deal with some general aspects that experience

confirms, e.g. the Hooke's law, the standard 2-parameter elastic isotropy at the macro scale, the decoupling between the hydrostatic and deviatoric response (Maxwell, 1853), the positivity of the elastic modules. This will be done also recalling the first proposition of the treatise of Love (1926): "The Mathematical Theory of Elasticity is occupied with an attempt to reduce to calculation the state of strain, or relative displacement, within a solid body which is subject to the action of an equilibrating system of forces...". By definitely broadening the initial restriction to purely central actions, as already proposed by Poisson and theorized by Voigt, it is allowed to develop the basic idea of an atomistic-molecular model in a geometric way which consists in maintaining a simple potential function \mathcal{U} , with additive form, being r_i the variation of length of a set of bonds:

$$\mathcal{U}(r_1, r_2, \dots) = F_1(r_1) + F_2(r_2) + \dots \quad (1)$$

This is a key point of the present modelling, numerically efficient as it can be managed by a diagonal constitutive operator.

2. Heuristic-molecules

2.1. Outline: configuration and displacements

This section presents the geometry and the bonds configuration of 4 basic heuristic molecules, or unit cells, which are plane. On the whole, the solid-model \mathcal{M} should be calculated at the macro-scale as a discrete assemblage of a finite number s of these UCs, that connect a number m of rigid elements.

The most basic scheme consists of a mechanistic model imagined as a discrete assemblage of rigid bodies, the idealized atoms, that are connected by central force bond-springs of positive stiffness. This "Central Force" scheme, (no-polar and monoatomic), is named CF-molecule, and implies the Cauchy-Poisson symmetries $C_{ijhk} = C_{ihjk}$ (Stakgold, 1950; Vannucci and Desmorat, 2016). Therefore in the isotropic case it results uni-constant, with a Poisson ratio $\nu = 0.25$ or $\nu = 0.33$ for plane strain and plane stress, respectively. In this case, the idealized atoms are simple material points, with no shape.

The second heuristic molecule consists of rigid bodies that are extended and have a specific shape in such a way as to interact more elaborately with their neighbors. The structure is inter-connected by "Central and Shear Forces", and thus named CSF-molecule, being able to exchange tangential shear forces, but not couples. In this case it will be possible to obtain a macroscopically isotropic behaviour even for values of $\nu \neq 0.25$, or $\nu \neq 0.33$.

The third and fourth heuristic molecules are evolutions of the previous one, since poles and bonds are added so that each atom can also exchange bending moments and further shear actions. They exhibit a behaviour that has a relation with a Cosserat solid continuum, and therefore are defined as "Central, Shear and Polar Force", CSPF-molecule, and Cosserat-molecule, respectively.

Dealing with plane solids, a plane Cartesian reference frame $\{O, \mathbf{e}^1, \mathbf{e}^2\}$ is fixed, and the location of the centre of the rigid bodies is given by node-points

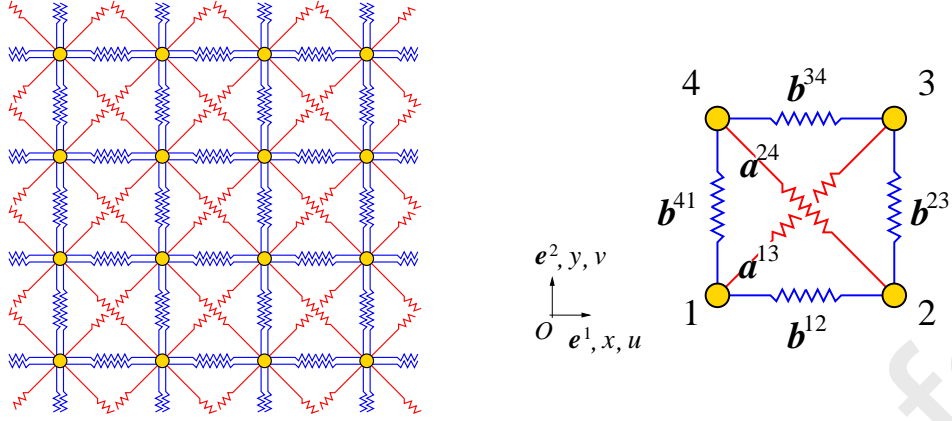


Figure 1: CF-molecule: Sketch of a global assemblage for a solid material model (left), and of a single unit cell (right).

in a Euclidean space \mathcal{E} to which a vector space is associated with the usual definition of inner product and length of a vector. Moreover, in general these rigid bodies have their proper spatial orientation defined by a local angle φ . Then, the initial placement of the solid-model \mathcal{M} is defined by the coordinates of each node $\{x^i, y^i\}_{i=1,m}$ and the angle φ^i , with $i = 1, \dots, m$, and assembled into the configuration matrices $[X]$ and $[\Phi]$ as follows

$$\begin{aligned} [X] &= \begin{bmatrix} x^1, x^2, \dots, x^m \\ y^1, y^2, \dots, y^m \end{bmatrix} \\ [\Phi] &= \begin{bmatrix} \varphi^1, \varphi^2, \dots, \varphi^m \end{bmatrix} \end{aligned} \quad (2)$$

The process of deformation from the initial reference configuration toward a displaced configuration $\chi(\mathcal{M}) = \mathcal{M}^\star$ is described by a mapping $\chi : [X] \mapsto [\mathbf{X}]^\star$, while the deformed configuration of the model is a function of the $3m$ Lagrangian coordinates $[U] = [\mathbf{X}]^\star - [X]$ and $[\Psi] = [\Phi]^\star - [\Phi]$. It is convenient to assemble the Lagrangian displacements $[U]$, $[\Psi]$, and the work-conjugate external nodal forces and couples $[P]$ as follows

$$\begin{aligned} [U] &= \begin{bmatrix} u^1, u^2, \dots, u^m \\ v^1, v^2, \dots, v^m \end{bmatrix}, & [P] &= \begin{bmatrix} p^1, p^2, \dots, p^m \\ q^1, q^2, \dots, q^m \\ \mu^1, \mu^2, \dots, \mu^m \end{bmatrix} \\ [\Psi] &= \begin{bmatrix} \psi^1, \psi^2, \dots, \psi^m \end{bmatrix} \end{aligned} \quad (3)$$

2.2. CF-molecule: only central forces

The most simple solid model made by four rigid bodies that are interconnected by central force bonds is shown in Fig. 1. The UC of the model is the square CF-molecule made by 4 atoms bonded together by 6 line-springs: 2 “**R**-red” bond-springs (\mathbf{a}^{ij}) that connect the opposite atoms along the diagonals and 4 “**B**-blue” bond-springs (\mathbf{b}^{ij}) along the sides that have an initial length

equal to $2e$. The absence of couple-effects is guaranteed by the convergence of the springs into the nodes, at the atoms' centre. A vector is associated to each bond-spring, and the components of these vectors are collected in the matrices $[D_a]$ and $[D_b]$ ¹ which are linearly related to the position of the barycentre of the atoms by the following bond relationship: ²

$$[\overset{\star}{D}_a | \overset{\star}{D}_b] = [\overset{\star}{X}] [L_a | L_b] \quad (4)$$

2.3. CSF-molecule: central and shear forces

The macroscopic behaviour of the most part of the solid materials adopted in engineering applications cannot be adequately described by a discrete model made by a regular mono-atomic lattice of "points and springs" in which there are only central forces (Voigt, 1887; Stakgold, 1950). This aspect is here overcome by adopting a mechanistic model which consist of a mono-atomic lattice of rigid bodies that have a "shape" and interacts also by means of "non-central", shear forces.

A visual sketch of the proposed mechanistic model is shown in Fig. 2. The UC of the CSF-molecule consists of 4 atoms bonded together by 10 line-springs that are of three different types. Fig. 3 shows the vectors that can be associated to these springs: the "*R*-red" and the "*B*-blue" bond-springs give the same central-force connection of the previous model, while the "*M*-magenta" spring gives the shear connection. An initial length f of the *M* bond-springs is shown here with the purpose of obtaining just a visual representation of the connection, for example by drawing the vector \mathbf{c}^{12} . In the subsequent algebraic formulation of the model the variation of length of this bond-spring will be divided by the length that corresponds to the distance between the connected atoms, that is $2e$, in order to obtain a measure of strain that is comparable with the usual shear strain in a continuum solid. Moreover, as far as the shear response is concerned, in the further development of the heuristic molecule that will be presented later, only the component of displacement orthogonal to the direction of the segment joining the barycentres of the connected atoms will be taken into account. The elongation of this shear spring, which connect

¹ being

$$[D_a] = \begin{bmatrix} a_x^{13} & a_x^{24} \\ a_y^{13} & a_y^{24} \end{bmatrix} \quad [D_b] = \begin{bmatrix} b_x^{12} & b_x^{23} & b_x^{34} & b_x^{41} \\ b_y^{12} & b_y^{23} & b_y^{34} & b_y^{41} \end{bmatrix}$$

² being

$$[L_a] = \begin{bmatrix} -1 & 0 \\ 0 & -1 \\ 1 & 0 \\ 0 & 1 \end{bmatrix} \quad [L_b] = \begin{bmatrix} -1 & 0 & 0 & 1 \\ 1 & -1 & 0 & 0 \\ 0 & 1 & -1 & 0 \\ 0 & 0 & 1 & -1 \end{bmatrix}$$

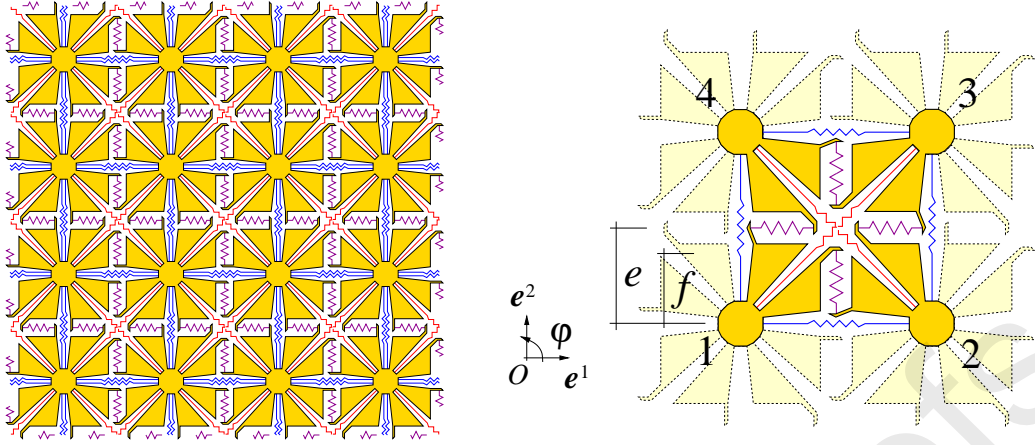


Figure 2: CSF-molecule: Sketch of a global assemblage for a plane solid material model (left), and of a single unit cell (right). The shape of the atoms is drawn for just an heuristic illustrative purpose, since the effective topology is given by Eq. (5) and subsequent linearization.

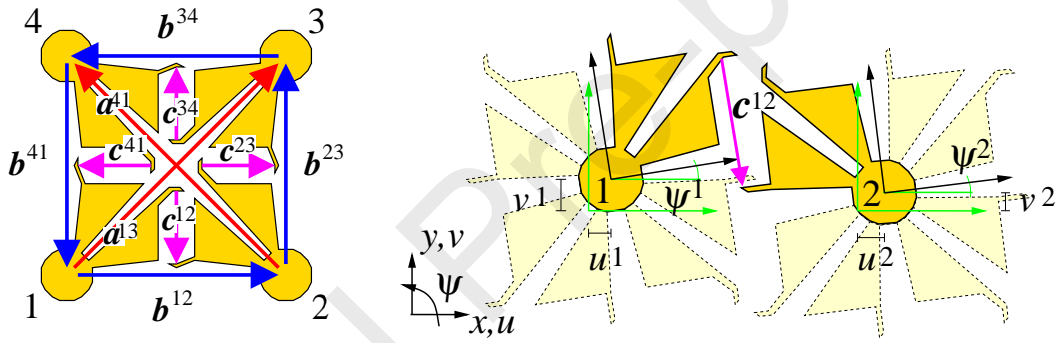


Figure 3: CSF-molecule: Unit cell for an isotropic no-polar solid material. Detail of the deformed shear link between the atoms 1-2.

the atoms $i - j$, depends both on the relative position of the baricentres of the atoms, as well as on the relative rotation between them. As an example, for the shear connection between atoms 1 – 2, shown in Figure 3, given the initial length of the magenta spring, equal to $f = e$, and the distance between the atoms, equal to $2e$, then the components of the spring-vector \mathbf{c}^{12} are given by:

$$\begin{Bmatrix} \star c_x^{12} \\ \star c_y^{12} \end{Bmatrix} = \begin{bmatrix} \star x_1 & \star x_2 \\ \star y_1 & \star y_2 \end{bmatrix} \begin{Bmatrix} -1 \\ 1 \end{Bmatrix} - \begin{bmatrix} \cos \psi^1 & -\sin \psi^1 \\ \sin \psi^1 & \cos \psi^1 \end{bmatrix} \begin{Bmatrix} e \\ f \end{Bmatrix} + \begin{bmatrix} \cos \psi^2 & -\sin \psi^2 \\ \sin \psi^2 & \cos \psi^2 \end{bmatrix} \begin{Bmatrix} -e \\ 0 \end{Bmatrix} \quad (5)$$

Thence, under the hypothesis of small displacements and rotations, and considering the case of an initial configuration such that $[\Phi] = [0]$ and $[\dot{\Phi}] = [\Psi]$, the components of these new 4 shear spring-vectors are obtained as a linear function of the configuration of the atoms by the following link relationship

$$[\dot{D}_c] = [\dot{X}][L_c] + [J_c] + [\Psi][G_c] \quad (6)$$

where the matrix $[\Psi]$, that contains the variation of rotation of the 4 atoms, has been rearranged as follows ³

$$[\Psi] = \begin{bmatrix} \psi^1 & \psi^2 & \psi^3 & \psi^4 & 0 & 0 & 0 & 0 \\ 0 & 0 & 0 & 0 & \psi^1 & \psi^2 & \psi^3 & \psi^4 \end{bmatrix} \quad (7)$$

90 2.4. CSPF-molecule: central, shear and polar forces

The third mechanistic model is an evolution of the previous mono-atomic UC, in which the **B**–blue springs are no more central with respect to the barycentre of the rigid bodies (or atoms). As a consequence, this heuristic CSPF-molecule gains the possibility to exert a bending moment between the rigid bodies connected by the **B**-blue bond-springs, and it can be related to an “enriched” continuum model, as already outlined in Casolo (2006). A sketch of this mechanistic model is shown in Figs. 4 and 5, with the purpose to grasp the topology of the present scheme. The UC consists of 4 atoms bonded together by 10 line-springs that are of three different types: the **R**–red springs give a central-force connection, the **B**–blue springs are non-central and thus give a bending moment and an axial connection which are coupled, while the **M**–magenta springs give the shear connection already described. In this case, the components \mathbf{b}^{12} of the axial non-central **B**–blue line-spring-vector connecting atoms 1 – 2, shown in Fig. 5, given the initial length g of the blue spring, are:

$$\begin{Bmatrix} \star_{b_x}^{12} \\ \star_{b_y}^{12} \end{Bmatrix} = \begin{bmatrix} \star_{x_1} & \star_{x_2} \\ \star_{y_1} & \star_{y_2} \end{bmatrix} \begin{Bmatrix} -1 \\ 1 \end{Bmatrix} - \begin{bmatrix} \cos \psi^1 & -\sin \psi^1 \\ \sin \psi^1 & \cos \psi^1 \end{bmatrix} \begin{Bmatrix} e-h \\ g \end{Bmatrix} + \begin{bmatrix} \cos \psi^2 & -\sin \psi^2 \\ \sin \psi^2 & \cos \psi^2 \end{bmatrix} \begin{Bmatrix} h-e \\ g \end{Bmatrix} \quad (8)$$

Under the hypothesis of small displacements and rotations, and considering the case of an initial configuration such that $[\Phi] = [0]$, and thus $[\Psi] = [\Phi]^\star$, then the components of the 4 **B**-blue bond-spring vectors are obtained as a linear function of the position and rotation of the atoms by the following link

³ the other matrices in the Eq. (6) are:

$$[D_c] = \begin{bmatrix} c_{x_1}^{12} & c_{x_2}^{23} & c_{x_3}^{34} & c_{x_4}^{41} \\ c_{y_1}^{12} & c_{y_2}^{23} & c_{y_3}^{34} & c_{y_4}^{41} \end{bmatrix} \quad [L_c] = \begin{bmatrix} -1 & 0 & 0 & 1 \\ 1 & -1 & 0 & 0 \\ 0 & 1 & -1 & 0 \\ 0 & 0 & 1 & -1 \end{bmatrix}$$

$$[J_c] = \begin{bmatrix} -2e & f & 2e & -f \\ -f & -2e & f & 2e \end{bmatrix} \quad [G_c] = \begin{bmatrix} f & 0 & 0 & -e \\ 0 & e & 0 & 0 \\ 0 & e & -f & 0 \\ 0 & 0 & 0 & -e \\ -e & 0 & 0 & 0 \\ -e & f & 0 & 0 \\ 0 & 0 & e & 0 \\ 0 & 0 & e & -f \end{bmatrix}$$

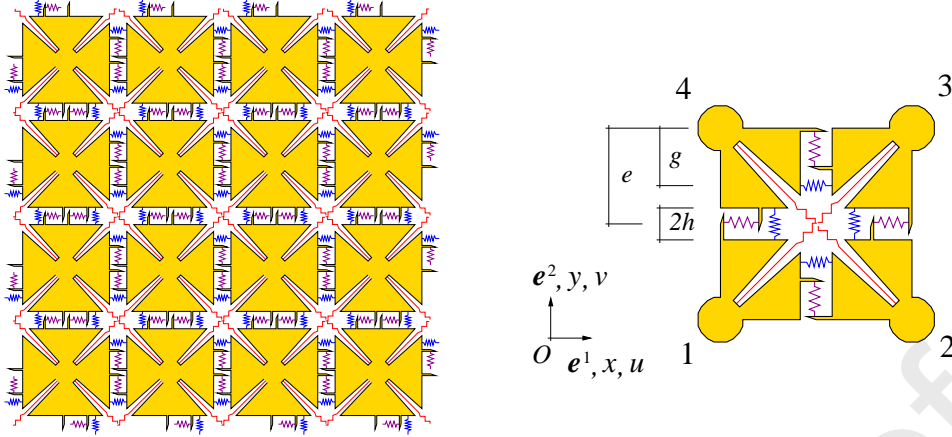


Figure 4: CSPF-molecule: Sketch of a global assemblage for a plane solid material model (left), and of a single unit cell (right). The shape of the atoms is drawn for an illustrative purpose, while the effective topology is given by the algebra according to Eq. (8) and subsequent linearization.

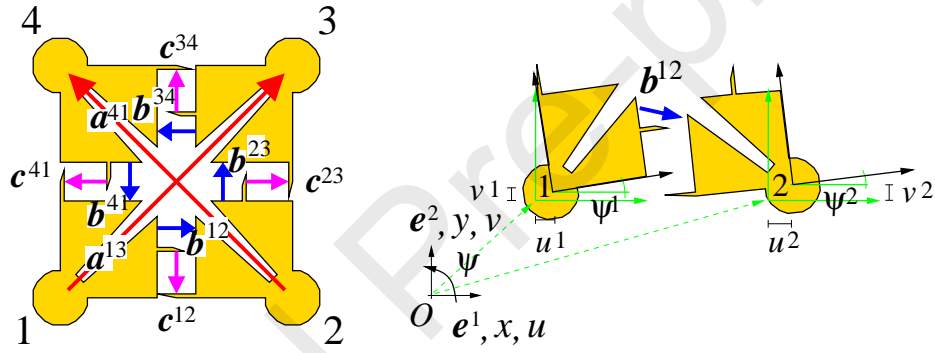


Figure 5: CSPF-molecule: Unit cell for an isotropic polar solid material. Detail of the deformed shear link between the atoms 1-2.

relationship ⁴

$$[\overset{\star}{D}_b] = [\overset{\star}{X}][\overset{\star}{L}_b] + [J_b] + [\Psi][G_b] \quad (9)$$

⁴ being;

$$[J_b] = \begin{bmatrix} 2(h-e) & 0 & 2(e-h) & 0 \\ 0 & 2(h-e) & 0 & 2(e-h) \end{bmatrix} \quad [G_b] = \begin{bmatrix} g & 0 & 0 & h-e \\ -g & e-h & 0 & 0 \\ 0 & e-h & -g & 0 \\ 0 & 0 & g & h-e \\ h-e & 0 & 0 & g \\ h-e & g & 0 & 0 \\ 0 & -g & e-h & 0 \\ 0 & 0 & e-h & -g \end{bmatrix}$$

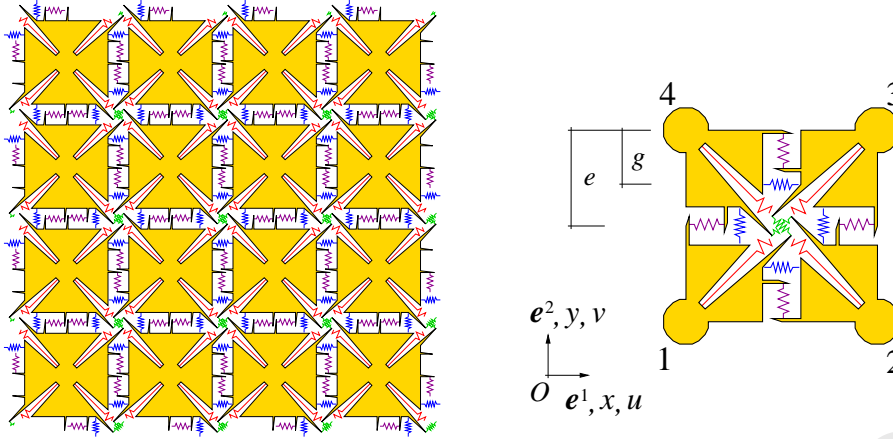


Figure 6: Cosserat-molecule: Sketch of a global assemblage for a plane solid material model (left), and of a single unit cell (right). In this case the unit cell is represented by only the 4 quarters of the atoms that compose the periodic element.

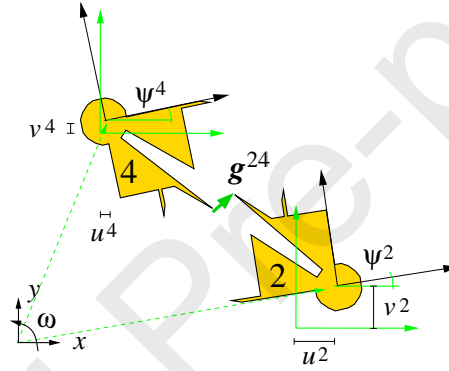


Figure 7: Cosserat-molecule: Detail of the deformed shear link between atoms 2-4.

2.5. An almost Cosserat-molecule

The fourth heuristic scheme is a further evolution, in which two “*G*-green” shear springs are added in order to connect the atoms along the diagonals of the previous heuristic-molecule. As a consequence, this scheme allows to couple also the diagonal atoms with a shear bonding that makes it possible to enhance the relationship of this discrete model to a more refined Cosserat continuum. A sketch of this mechanistic model is shown in Figs. 6-7. An assemblage of 16 atoms is shown on the left side of Fig. 6, while a periodic UC is drawn in the right side, consisting of 4 quarter of atoms bonded together by the 12 line-springs that are of four different types: the *R*-red springs give a central-force connection, the *B*-blue springs are non-central and thus create a bending moment and axial connection that are coupled, while the *M*-magenta and the *G*-green springs create the shear connections along the sides and the diagonals, respectively. For the purpose of the present manuscript, a linear relation is also assumed for the strain of the *G*-green bond spring, which consists of the ratio between the elongation of this spring along the normal direction with respect

to the diagonal segment, over the full distance of the atoms connected along the diagonal in the initial configuration.

3. Deformation and strain of the bonds

110 3.1. Rotation indifference

The measure of length of the bond-springs that is built by using the square of the modulus of the vectors associated to the bond-springs is indifferent with respect to an orthogonal transformation $[Q]$. As an example, consider Eqs. (8,9) and then:

$$\{\dot{b}_Q\}^{\star ij} = [Q][\dot{X}]\{l^{ij}\} - [Q][R(\psi^i)]\{g^{ij}\} + [Q][R(\psi^j)]\{g^{ji}\} \quad (10)$$

$$[\dot{D}_{bQ}]^{\star} = [Q][\dot{X}][L_b] + [Q][J_b] + [Q][\Psi][G_b] \quad (11)$$

and consequently, respectively:

$$\{\dot{b}_Q\}^{\star ij T} \{\dot{b}_Q\}^{\star ij} = \{\dot{b}\}^{\star ij T} [Q]^T [Q] \{\dot{b}\}^{\star ij} = \{\dot{b}\}^{\star ij T} \{\dot{b}\}^{\star ij} \quad (12)$$

$$[\dot{D}_{bQ}]^{\star T} [\dot{D}_{bQ}]^{\star} = [\dot{D}_b]^{\star T} [Q]^T [Q] [\dot{D}_b]^{\star} = [\dot{D}_b]^{\star T} [\dot{D}_b]^{\star} \quad (13)$$

3.2. Strain measure

The strain measure for the heuristic molecules is based on the changes of length of the inter-atomic links in the process of deformation $\chi : \mathcal{M} \mapsto \dot{\mathcal{M}}$. Suppose that $[\Phi] = [0]$ initially, then the relationship between the components of the elongation of the bond-springs and the Lagrangian displacements, $[U]$, $[\Psi]$ is:

$$\begin{aligned} [\dot{D}]^{\star} &= [\dot{X}][L] + [J] + [\Psi][G] \\ [D] &= [X][L] + [J] \\ [\Delta] &= [\dot{D}]^{\star} - [D] = [U][L] + [\Psi][G] \end{aligned} \quad (14)$$

The lengths of the bond-springs, in the initial reference and in the deformed configuration, are calculated and assembled in two vectors $\{d\}$ and $\{\dot{d}\}^{\star}$ respectively, as follows ⁵

$$\begin{aligned} \{d\} &= \text{diag}([D]^T [D])^{1/2} \\ \{\dot{d}\}^{\star} &= \text{diag}([\dot{D}]^{\star T} [\dot{D}]^{\star})^{1/2} \end{aligned} \quad (15)$$

⁵ $\text{diag}[A]$ returns a column vector formed from the elements of the main diagonal of square matrix $[A]$, while $\text{Diag}\{a\}$, where $\{a\}$ is a vector with n components, returns an $n \times n$ diagonal matrix having $\{a\}$ as its main diagonal.

The scalar components d_i can be used to build a measure of strain since they are insensitive to orthogonal transformation, as shown in Sec. 3.1. The bond-springs' Green-Lagrange strain and an Engineering strain can then be evaluated and assembled in a vector $\{\varepsilon^L\}$ and in a vector $\{\varepsilon^E\}$, respectively, as follows

$$\{\varepsilon^L\} = \frac{1}{2} \left(\{d\}^{\star 2} - \{d\}^2 \right) \text{Diag} \{d\}^{-2} \quad (16)$$

$$\{\varepsilon^E\} = \left(\{d\}^{\star} - \{d\} \right) \text{Diag} \{d\}^{-1} \quad (17)$$

A linearized measure of strain $\{\varepsilon\}$ can also be obtained from the Lagrangian strains with the following procedure under the hypothesis of small displacements ($u^i, v^i \ll 2e$) around the reference configuration:

$$\begin{aligned} \text{Diag}\{\varepsilon^L\} &= \frac{1}{2} \left([\dot{D}]^T [\dot{D}] - [D]^T [D] \right) \cdot \text{Diag} \{d\}^{-2} = \\ &\simeq \text{sym}([\Delta]^T [D]) \cdot \text{Diag} \{d\}^{-2} = \text{Diag}\{\varepsilon\} \end{aligned} \quad (18)$$

The strain measure ε is then associated to each bond-spring, which is simply the first order term of the change in the bond length divided by the original inter-atomic distance. In many cases, given the linearity of $[\Delta]$ with respect to the displacements, it can be practical to rewrite the last relation, by rearranging the displacements into a vector $\{u\}$ and by assembling a strain-displacement matrix $[B]$ for a given molecule, as follows ⁶

$$\{\varepsilon\} = [B] \{u\} \quad (20)$$

On the other hand, to study the case of meta-materials governed by a kinematics where the displacements can no longer be considered small, such as the pantographic lattices and structures (Dell'Isola et al., 2016; Turco et al., 2016), it will be necessary to resort to a full non-linear kinematics.

⁶ As an example, the linearized strain-displacement relation $\{\varepsilon\} = [B]\{u\}$ for the Cosserat heuristic-molecule shown in Fig. 6 is

$$\begin{pmatrix} \varepsilon_{13}^R \\ \varepsilon_{14}^R \\ \varepsilon_{24}^B \\ \varepsilon_{12}^B \\ \varepsilon_{23}^B \\ \varepsilon_{34}^B \\ \varepsilon_{41}^B \\ \gamma_{13}^G \\ \gamma_{14}^G \\ \gamma_{24}^M \\ \gamma_{12}^M \\ \gamma_{23}^M \\ \gamma_{34}^M \\ \gamma_{41}^M \end{pmatrix} = \frac{1}{4e} \begin{bmatrix} -1 & -1 & 0 & 0 & 0 & 0 & 1 & 1 & 0 & 0 & 0 & 0 \\ 0 & 0 & 0 & 1 & -1 & 0 & 0 & 0 & 0 & -1 & 1 & 0 \\ -2 & 0 & 2g & 2 & 0 & -2g & 0 & 0 & 0 & 0 & 0 & 0 \\ 0 & 0 & 0 & 0 & -2 & 2g & 0 & 2 & -2g & 0 & 0 & 0 \\ 0 & 0 & 0 & 0 & 0 & 0 & 2 & 0 & 2g & -2 & 0 & -2g \\ 0 & -2 & -2g & 0 & 0 & 0 & 0 & 0 & 0 & 0 & 2 & 2g \\ 1 & -1 & -2e & 0 & 0 & 0 & -1 & 1 & -2e & 0 & 0 & 0 \\ 0 & 0 & 0 & 1 & 1 & -2e & 0 & 0 & 0 & -1 & -1 & -2e \\ 0 & 2 & 2e & 0 & -2 & 2e & 0 & 0 & 0 & 0 & 0 & 0 \\ 0 & 0 & 0 & -2 & 0 & 2e & 2 & 0 & 2e & 0 & 0 & 0 \\ 0 & 0 & 0 & 0 & 0 & 0 & 0 & -2 & 2e & 0 & 2 & 2e \\ -2 & 0 & 2e & 0 & 0 & 0 & 0 & 0 & 0 & 2 & 0 & 2e \end{bmatrix} \begin{pmatrix} u^1 \\ v^1 \\ \psi^1 \\ u^2 \\ v^2 \\ \psi^2 \\ u^3 \\ v^3 \\ \psi^3 \\ u^4 \\ v^4 \\ \psi^4 \end{pmatrix} \quad (19)$$

3.3. Strain energy

The strain energy of the heuristic-molecule model, is defined according to the spirit of an idealized spring-like interatomic bond, as schematized in Fig. 8. Equilibrium and stability of each bond in the reference configuration ($a = a_0$), in the absence of pre-stress, require the following conditions for the potential energy \mathcal{U}_a

$$\left. \frac{d\mathcal{U}_a}{da} \right|_{a_0} = F = 0 \quad , \quad \left. \frac{d^2\mathcal{U}_a}{da^2} \right|_{a_0} = c > 0 \quad (21)$$

where c is the stiffness of the bond, assumed as constant for small stretching around the reference configuration, according with Hooke's law. Thus, the variation of strain energy \mathcal{U}_ε of the solid-model from the initial stable reference placement \mathcal{M} to \mathcal{M}^\star is a quadratic function of the strains. Given the elastic stiffnesses of all the inter-atomic links, which are assembled in a diagonal elasticity matrix $[C] = \text{Diag}\{c\}$, and given Eqs. (18-20) to define the kinematics, then strain energy is directly related to the Lagrangian coordinates $[U] \sim \{u\}$

$$\mathcal{U}_\varepsilon = \frac{1}{2} \{u\}^T [B]^T [C] [V] [B] \{u\} = \frac{1}{2} \{u\}^T [K] \{u\} \quad (22)$$

being $[K]$ the symmetric stiffness matrix of the numerical model, while $[V]$ is the diagonal matrix which contains the volume of the UC.

4. Bond-springs elasticity

4.1. Elasticity of the CF-molecule

The CF molecule has 2 types of bond-spring stiffnesses that should be determined, the *R*-red and the *B*-blue ones (c_R , c_B) as shown in Fig. 1. Thus, the strain energy that corresponds to two independent homogeneous displacement gradient fields, \mathbf{H}^H and \mathbf{H}^D (hydrostatic and deviatoric, respectively), are considered:

$$\begin{aligned} \mathbf{H}^H &= \epsilon (\mathbf{e}^1 \otimes \mathbf{e}^1 + \mathbf{e}^2 \otimes \mathbf{e}^2) \\ \mathbf{H}^D &= \epsilon (\mathbf{e}^1 \otimes \mathbf{e}^2 + \mathbf{e}^2 \otimes \mathbf{e}^1) \end{aligned} \quad (23)$$

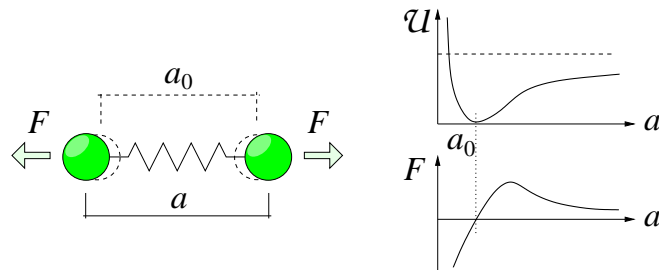


Figure 8: Schematic spring-like bond between two atoms (left); potential energy and force-distance curves (right).

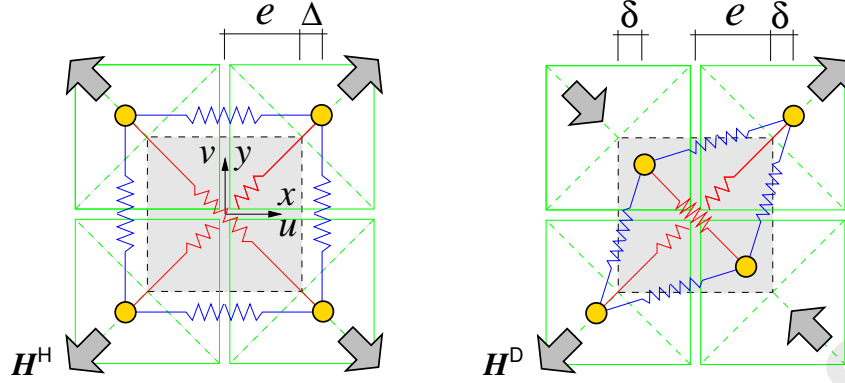


Figure 9: Deformed CF-molecule: Hydrostatic and deviatoric configuration.

being $\epsilon = \delta/e$. The corresponding deformed configuration of the CF-molecule is shown in Fig. 9. In this case, the hydrostatic and deviatoric Green-Lagrange measure of strain assigned to the bond-springs are respectively

$$\begin{aligned} \{\mathcal{E}^H\}^T &= \{\epsilon, \epsilon, \epsilon, \epsilon, \epsilon, \epsilon\} \left(1 + \frac{\epsilon}{2}\right) \\ \{\mathcal{E}^D\}^T &= \left\{\epsilon + \frac{\epsilon^2}{2}, -\epsilon + \frac{\epsilon^2}{2}, \frac{\epsilon^2}{2}, \frac{\epsilon^2}{2}, \frac{\epsilon^2}{2}, \frac{\epsilon^2}{2}\right\} \end{aligned} \quad (24)$$

and the linear part of this strain measure is simply:

$$\begin{aligned} \{\mathcal{E}^H\}^T &= \{\epsilon, \epsilon, \epsilon, \epsilon, \epsilon, \epsilon\} \\ \{\mathcal{E}^D\}^T &= \{\epsilon, -\epsilon, 0, 0, 0, 0\} \end{aligned} \quad (25)$$

while the elastic moduli of the corresponding bond-springs are assembled in vector

$$\{\text{diag}[C]\}^T = \{c^R, c^R, c^B, c^B, c^B, c^B\} \quad (26)$$

In what follows, a linear assumption is made for the elastic energy density $\mathcal{U}_{\text{CF}} = \frac{1}{2}\{\epsilon\}^T[C]\{\epsilon\}$, in a corresponding UC, according to Eq. (22), which gives:

$$\begin{aligned} \mathcal{U}_{\text{CF}}^H &= (c^R + 2c^B) \epsilon^2 \\ \mathcal{U}_{\text{CF}}^D &= c^R \epsilon^2 \end{aligned} \quad (27)$$

4.1.1. CF-relationship with the isotropic Cauchy continuum

The relationship between the present heuristic model and the isotropic Cauchy continuum is developed by comparison in terms of displacement field and strain energy density. Given a fixed reference configuration, the deformation of the continuum solid body \mathcal{B} is described by a smooth homeomorphism $\chi(\mathcal{B})$, with $\det \nabla \chi > 0$. The displacement of a material point \mathbf{x} , the deformation gradient \mathbf{F} , and the displacement gradient \mathbf{H} are given respectively by

$$\begin{aligned} \mathbf{u}(\mathbf{x}) &= \chi(\mathbf{x}) - \mathbf{x} \\ \mathbf{F} &= \nabla \chi \\ \mathbf{H} &= \nabla \mathbf{u} = \mathbf{F} - \mathbf{I} \end{aligned} \quad (28)$$

The infinitesimal strain tensor is $\mathbf{E} = \text{sym}\mathbf{H}$, while $\mathbf{W} = \text{skw}\mathbf{H}$ characterizes the macro-rotation in the case of small $\|\mathbf{H}\|$. In the present manuscript, the case of a plane linear-elastic solid body is considered, for which:

$$\mathcal{U} = \frac{1}{2} \{E\}^T [\mathbf{C}] \{E\} \quad (29)$$

having collected the components of the infinitesimal deformation as follows

$$\{E\}^T = \{ E_{11}, E_{22}, E_{12}, E_{21} \} \quad (30)$$

while the elasticity matrices based on the hypothesis of plane strain $[\mathbf{C}_E]$, and of plane stress $[\mathbf{C}_S]$ are, respectively

$$[\mathbf{C}_E] = 2G \begin{bmatrix} \frac{1-\nu}{1-2\nu} & \frac{\nu}{1-2\nu} & 0 & 0 \\ \frac{\nu}{1-2\nu} & \frac{1-\nu}{1-2\nu} & 0 & 0 \\ 0 & 0 & \frac{1}{2} & \frac{1}{2} \\ 0 & 0 & \frac{1}{2} & \frac{1}{2} \end{bmatrix}, \quad [\mathbf{C}_S] = 2G \begin{bmatrix} \frac{1}{1-\nu} & \frac{\nu}{1-\nu} & 0 & 0 \\ \frac{\nu}{1-\nu} & \frac{1}{1-\nu} & 0 & 0 \\ 0 & 0 & \frac{1}{2} & \frac{1}{2} \\ 0 & 0 & \frac{1}{2} & \frac{1}{2} \end{bmatrix} \quad (31)$$

where G is the shear modulus. The corresponding density of strain energies are:

$$\begin{aligned} \mathcal{U}_E^H &= \frac{2G}{1-2\nu} \epsilon^2, & \mathcal{U}_S^H &= \frac{2G(1+\nu)}{1-\nu} \epsilon^2 \\ \mathcal{U}_E^D &= 2G \epsilon^2, & \mathcal{U}_S^D &= 2G \epsilon^2 \end{aligned} \quad (32)$$

where the subscripts **E** and **S** refer to the plane strain and plane stress respectively, while the superscripts **H** and **D** refer to the hydrostatic or deviatoric field. The values of the stiffness modulus assigned to the **R**-red and **B**-blue bond-springs are obtained by comparing Eqs. (27) and (32)

$$\begin{aligned} c_E^R &= 2G, & c_S^R &= 2G \\ c_E^B &= \frac{2\nu}{1-2\nu} G, & c_S^B &= \frac{2\nu}{1-\nu} G \end{aligned} \quad (33)$$

For $\nu = 0$ the **B**-blue bond-spring vanishes, while for $\nu \rightarrow 0.5$ the **B**-blue spring tends to become fully rigid in the plane strain case. It is worth noting from Eqs. (33) that, in the case of plane strain, the CF model requires $G > 0$ and $\nu \in (0, \frac{1}{2})$ in order to have positive values of the strain energy and of the spring stiffness. On the other hand, the corresponding range of the Poisson ratio is $\nu \in (0, 1)$ for the plane stress case. In more detail, for $\nu = 0.25$ all the atoms are bonded by a unique type of spring, being $c^R = 2c^B = 2G$ for the plane strain case, while the same situation happens for $\nu = \frac{1}{3}$ in the case of plane stress.

A graphical synthesis of the response of this topology in terms of anisotropy is shown in Fig. 4.1.1 that reports the ratio of the strain energy density stored in a molecule, $\mathcal{U}(\theta)/\mathcal{U}(0)$, when subjected to a given deformation which is rotated at angle θ with respect to the principal reference system: $\mathbf{F}(\theta) = \mathbf{R}(\theta)\mathbf{F}\mathbf{R}^T(\theta)$, being

$$[\mathbf{R}(\theta)] = \begin{bmatrix} \cos(\theta) & -\sin(\theta) \\ \sin(\theta) & \cos(\theta) \end{bmatrix} \quad (34)$$

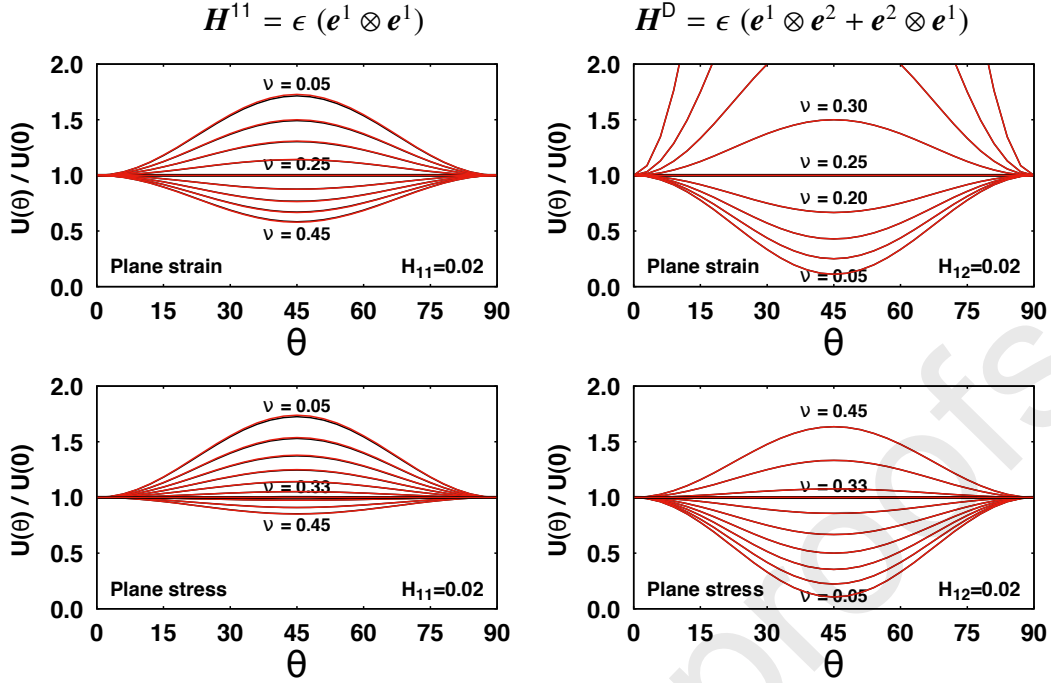


Figure 10: Anisotropy of the CF-molecule. Ratio of the elastic energy density $\mathcal{U}(\theta)/\mathcal{U}(0)$ as a function of the rotation of the displacement field. Different values of Poisson ratio (at steps of 0.05) have been considered. The red lines correspond to the Lagrangian strain measure while the black ones to the engineering strain measure, which are quite identical and in the drawings they appear almost coincident.

Two measures of strain have been used to evaluate the elastic energy: i) the Lagrangian strain evaluated according to Eq. (16), and ii) the engineering strain according to Eq. (17). The corresponding red lines and the black lines shown in Figure 4.1.1, which are superimposed and almost identical, report the response adopting the Lagrangian and the engineering strain respectively. The response is isotropic only for $\nu = 0.25$ when evaluating the elastic constants according with the plane strain hypothesis, while the isotropy is obtained for $\nu = \frac{1}{3}$ when evaluating the elastic constants according with the plane stress hypothesis. The approximation to the isotropic response is better, on average, with the c_S^B and c_S^R elastic constants. In this case it is acceptable for a restricted range around $\nu = \frac{1}{3}$, but becomes progressively bad when ν is outside the range (0.25 – 0.40).

4.2. Elasticity of the CFS-molecule

The measure of strain associated to each bond-spring of a UC of CFS type is assembled in the following vector:

$$\{\varepsilon_{\text{CSF}}\}^T = \{\varepsilon_{13}^R, \varepsilon_{24}^R, \varepsilon_{12}^B, \varepsilon_{23}^B, \varepsilon_{34}^B, \varepsilon_{41}^B, \gamma_{12}^M, \gamma_{23}^M, \gamma_{34}^M, \gamma_{41}^M\} \quad (35)$$

The strain components γ_{ij}^M associated to the M -magenta bond-springs are obtained by dividing the variation of length of the shear connection by the distance $2e$ of the atoms i and j . A third equation, that balances also the strain energy density for the case of a simple horizontal elongation, $\mathbf{H}^{11} = \epsilon (\mathbf{e}^1 \otimes \mathbf{e}^1)$ is needed to assign the values of stiffness to the three types of bond-springs. Thence, the three cases, for a CFS-molecule subjected to the corresponding deformations are shown in Figure 11. The linearized strain measures associated to the bond-springs for the hydrostatic, deviatoric and uniaxial elongation are respectively:

$$\begin{aligned} \{\varepsilon^H\}^T &= \{\epsilon, \epsilon, \epsilon, \epsilon, \epsilon, \epsilon, 0, 0, 0, 0\} \\ \{\varepsilon^D\}^T &= \{\epsilon, -\epsilon, 0, 0, 0, 0, -\epsilon, \epsilon, -\epsilon, \epsilon\} \\ \{\varepsilon^{11}\}^T &= \{\epsilon/2, \epsilon/2, \epsilon, 0, \epsilon, 0, 0, 0, 0, 0\} \end{aligned} \quad (36)$$

The elastic moduli of the corresponding CSF bond-springs are assembled in

$$\{\text{diag}[C]\}^T = \{c^R, c^R, c^B, c^B, c^B, c^B, c^M, c^M, c^M, c^M\} \quad (37)$$

Then, the elastic energy densities in the unit cell, according to the linear assumption for the strain expressed by Eq. (36) are:

$$\begin{aligned} \mathcal{U}_{\text{CSF}}^H &= (c^R + 2c^B) \epsilon^2 \\ \mathcal{U}_{\text{CSF}}^D &= (c^R + 2c^M) \epsilon^2 \\ \mathcal{U}_{\text{CSF}}^{11} &= (\frac{1}{4}c^R + c^B) \epsilon^2 \end{aligned} \quad (38)$$

4.2.1. CSF-relationship with the isotropic Cauchy continuum

Similarly to the previous CF case, the elastic energy densities given in Eq. (38) are balanced with those of a continuum Cauchy material in plane strain or plane stress condition already given by Eqs. (32), to which the following case of a uniform uniaxial tensile strain should be added:

$$\mathcal{U}_E^{11} = \frac{1-\nu}{1-2\nu} G\epsilon^2, \quad \mathcal{U}_S^{11} = \frac{1}{1-\nu} G\epsilon^2 \quad (39)$$

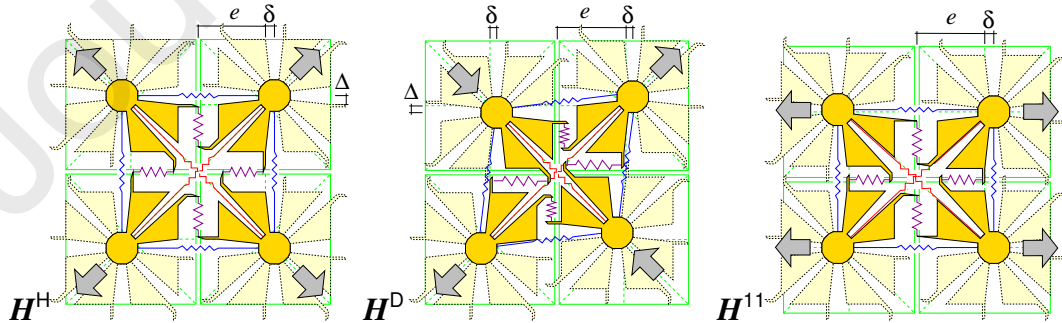


Figure 11: Deformed CSF-molecule: Hydrostatic, deviatoric and uniaxial deformation.

As a result, the following values of the elastic moduli of the red, blue and magenta CSF bond-springs are computed:

$$\begin{aligned} c_E^R &= \frac{4\nu}{1-2\nu} G & , & & c_S^R &= \frac{4\nu}{1-\nu} G \\ c_E^B &= G & , & & c_S^B &= G \\ c_E^M &= \frac{1-4\nu}{1-2\nu} G & , & & c_S^M &= \frac{1-3\nu}{1-\nu} G \end{aligned} \quad (40)$$

As a first observation, it is noticeable that for $\nu = 0$ the diagonal “*R*-red” bond-spring vanishes for both the plane strain and the plane stress cases. On the other hand, the “*M*-magenta” vanishes for $\nu = \frac{1}{4}$ for the plane strain case, while it vanishes for $\nu = \frac{1}{3}$ in the case of plane stress. Moreover, this CSF model requires $G > 0$ and $\nu \in (0, \frac{1}{4})$ in order to have positive values of the strain energy as well as of the spring stiffness in the case of plane strain, while the range of the Poisson ratio should be $\nu \in (0, \frac{1}{3})$ for the plane stress case.

A graphical synthesis of the response of this UC arrangement in terms of anisotropy is shown in Fig. 12 that reports the ratio of the strain energy stored in a CSF molecule, $\mathcal{U}(\theta)/\mathcal{U}(0)$, when subjected to a given deformation which is rotated at angle θ with respect to the principal reference system. Given the values of the elastic characteristics of the bond-springs (Eq. 40), the results obtained by adopting three measures of strain, for the bond-springs of the CSF molecule subjected to the deformation at different angles, are shown in Fig. 12: i) the almost Lagrangian strain evaluated according to Eq. (16), with the red lines, ii) the engineering strain according to Eq. (17), with the blue lines, and iii) the measure, called RBSM, that combines the engineering strain for the *R*-red bond-springs, while for the *B*-blue bond-springs the measure is the ratio of their elongation projected along the initial direction of the spring over the initial distance of the atoms (plotted with the black lines).

The first measure is named “almost Lagrangian strain” because the strain assumed for the *M*-magenta bond-springs is always the ratio of their elongation projected along the initial direction of the spring over the initial distance of the atoms. The third measure is substantially inspired to the measure already assumed in a previous rigid body-spring model (RBSM) (Casolo, 2004).

These graphs show that the CSF molecule is almost isotropic for small displacements. The very small variations of the elastic energy that corresponds to different angles of deformation are functions of the magnitude of the deformation factor ϵ , with the trend shown in the Figure 13. It is worth observing that the response to a deviatoric strain remains always perfectly isotropic when assuming the almost Lagrangian strain.

The trends of the ratio of the *R*-red and *M*-magenta bond-springs stiffnesses over the *B*-blue bond-spring stiffness are shown in Figure 14. The two series of plots report the case of plane strain and plane stress respectively. It is worth noting that in the case of $\nu = 0$ the CSF heuristic molecule without the diagonal *R*-red bond-springs has an isotropic response, which recalls the RBSM model already proposed by Casolo (2004, 2009). On the other hand, the cases

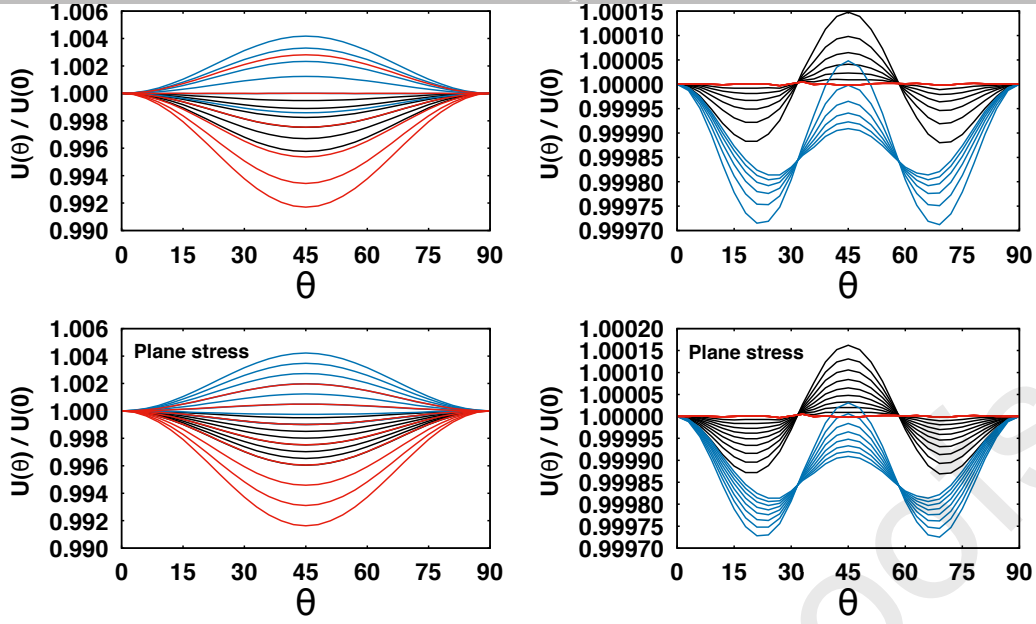


Figure 12: Isotropy of CSF molecule: Plot of the ratio $U(\theta)/U(0)$, of the elastic energy evaluated for a deformation field applied at different orientation θ , over the elastic energy corresponding to the deformation at $\theta = 0^\circ$. Left: uniaxial tensile deformation; Right column: pure deviatoric deformation. Red lines refer to the almost Lagrange strain measure, blue lines to the engineering measure, and black lines refer to the RBSM strain measure. Each line corresponds to a different Poisson ratio ν ($0 \rightarrow 0.25$ for plane strain, $0 \rightarrow 0.33$ for plane stress, with step of 0.05).

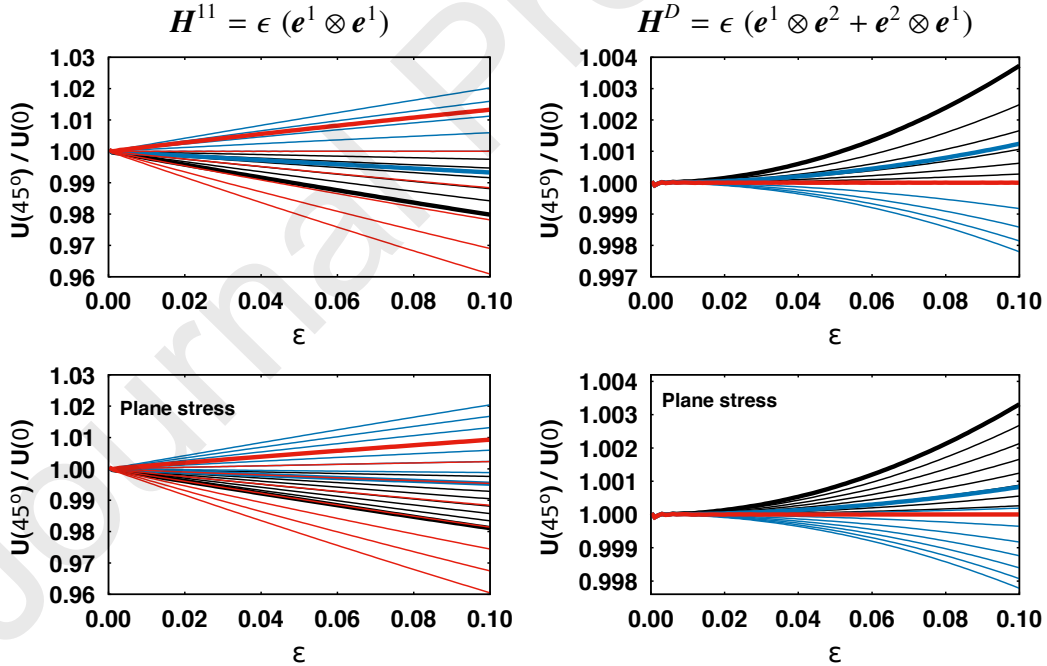


Figure 13: Numerical evidence of the approximation error due to the rotation of 45° of the deformation as a function of the amplitude of the displacement. Left column: uniaxial tensile deformation; Right column: pure deviatoric deformation. Red lines refer to the almost Lagrange strain measure, blue lines to the engineering measure, and black lines refer to the RBSM strain measure. The thickest lines correspond to the case of $\nu = \frac{1}{4}$ and $\nu = \frac{1}{3}$ for plane strain and plane stress, respectively.

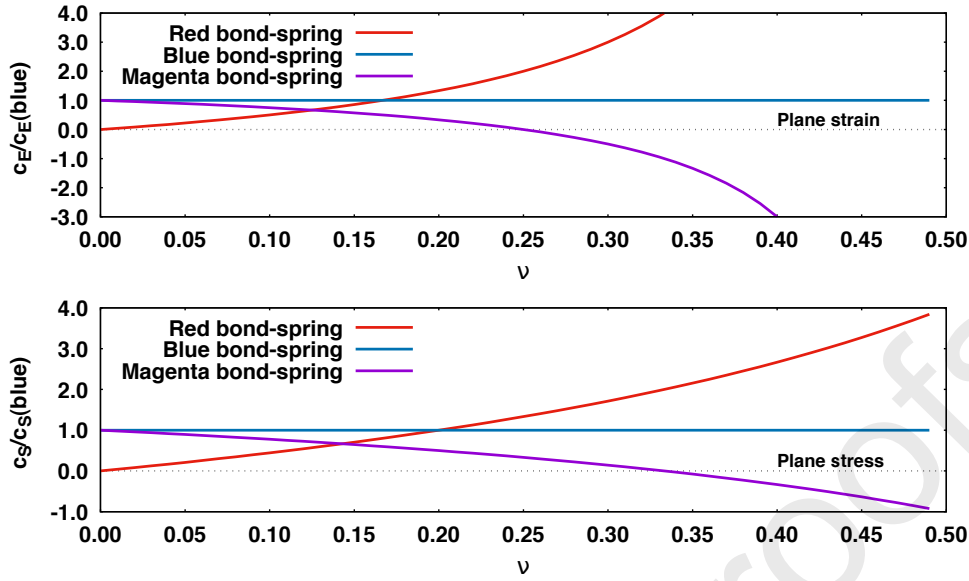


Figure 14: CSF molecule: Trends of the stiffness ratio of the different bond-spring as a function of the Poisson ratio ν . All the stiffnesses are normalized with respect to the stiffness of the *B*-blue bond-spring.

of $\nu = \frac{1}{4}$ (for the plane strain) and $\nu = \frac{1}{3}$ (for the plane stress) require that the shear bond-springs (*M*-magenta) should vanish and thus these UCs fall into the form of the CF heuristic molecule examined in the previous section 4.1.1. It is worth noting that the negative stiffness of the *M*-magenta bond-springs, for $\nu > \frac{1}{4}$ and for $\nu > \frac{1}{3}$ in the case of plane strain and plane stress, respectively, is in accord to what already reported by Diana and Casolo (2019), and Zhao and Zhao (2012), which also gave a physical interpretation based on the shape of the potential functions used in MD simulations of the distinct lattice spring modelling of the structure of silver.

4.3. Elasticity of the CSPF-molecule

The heuristic CSPF-molecule contains a polar interaction between the atoms which is obtained by adding a lateral separation, the distance g , to the pair of *B*-blue bond-springs at each side, as shown in the example of Figure 4. In solid mechanics applications, a behaviour of this type is often associated to a highly heterogeneous solid with a periodic internal structure. In this case, a representative volume, RVE, of the heterogeneous material is considered and an internal angular variable can be adopted in the continuum homogenization to represent the orientation of the more rigid subdomain of the RVE.

The CSPF-molecule can thus be related to a continuum with an enriched kinematics which includes a gradient of the material micro-rotation field ω . When considering the case of a Cosserat plane solid continuum, making refer-

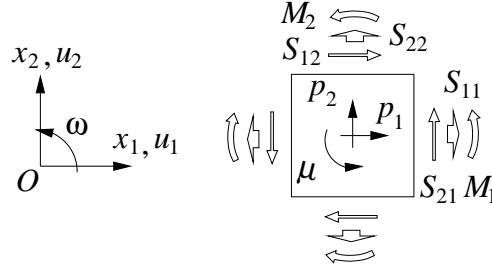


Figure 15: Notation adopted for the plane Cosserat continuum.

ence to the symbols shown in Fig. 15, two displacements $\{u_1, u_2\}$ and a local rotation ω are associated to each point, while $S_{\alpha\beta}$ and M_α are the components of the stress and couple stress tensor, respectively. The field equations and the boundary conditions are:

$$\begin{cases} S_{\alpha\beta, \beta} + p_\alpha = 0 \\ M_{\alpha, \alpha} + \epsilon_{3\alpha\beta} S_{\beta\alpha} + \mu = 0 \end{cases} \quad \text{in } \Omega \quad (41)$$

$$\begin{cases} S_{\alpha\beta} n_\beta - s_\alpha = 0 \\ M_\alpha n_\alpha - m = 0 \end{cases} \quad \text{on } \partial\Omega$$

where ϵ_{ijk} is the alternating symbol; p_α and μ are respectively the body forces and the body couple; n_1, n_2 are the components of the outward unit normal to the boundary $\partial\Omega$; s_α and m are the prescribed tractions and couples; $\alpha, \beta = 1, 2$. Summation of repeated indexes is implicit. The strains, conjugated in virtual work to these stress and the couple stress tensors, are given by the tensors $E_{\alpha\beta}$ and K_α which are function of the displacements and the micro-rotation

$$\begin{aligned} E_{\alpha\beta} &= u_{\alpha, \beta} + \epsilon_{3\alpha\beta} \omega_3 \\ K_\alpha &= \omega_{, \alpha} \end{aligned} \quad (42)$$

being $\alpha, \beta = 1, 2$. The Eq. (42) shows that the shear strains are not necessarily symmetric as they are affected by the micro-rotation ω , and for $\alpha \neq \beta$ it is worth to distinguish a “symmetric shear strain” E_s , a “macro-rotation” E_w , and a “relative micro-rotation” E_ω as follows (see Figure 16, from Casolo (2006)):

$$\begin{aligned} E_s &= \frac{1}{2} (u_{1,2} + u_{2,1}) \\ E_w &= \frac{1}{2} (-u_{1,2} + u_{2,1}) \\ E_\omega &= E_w - \omega \end{aligned} \left\} \rightarrow \begin{cases} E_{12} = E_s - E_\omega \\ E_{21} = E_s + E_\omega \end{cases} \quad (43)$$

The two deformation schemes that are shown in Figure 17 should also be considered for this heuristic molecule model. The case of a uniform micro-rotation is shown on the left side, where the size of the UC is set equal to hypothetical periodic material that corresponds to the enriched continuum. Under the hypothesis of a very small deformation $\omega = \varphi \ll 1$, only the M -magenta bond springs are deformed and thus

$$\{\epsilon^\Omega\}^T = \{0, 0, 0, 0, 0, 0, \omega, \omega, \omega, \omega\} \quad (44)$$

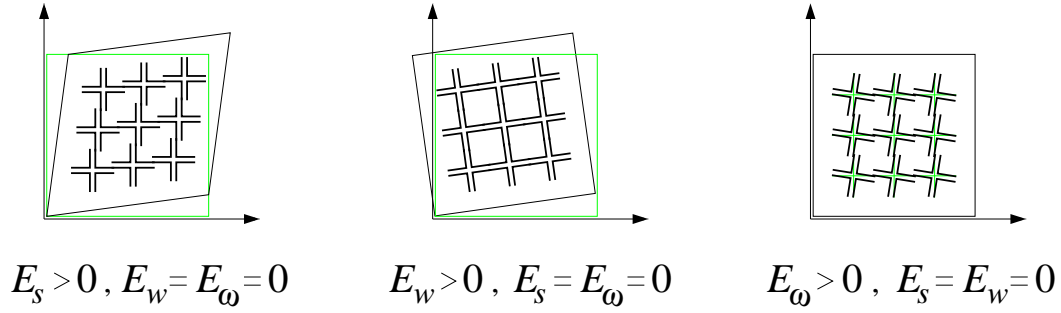


Figure 16: Heuristic interpretation of simple deformations for a plane Cosserat continuum.

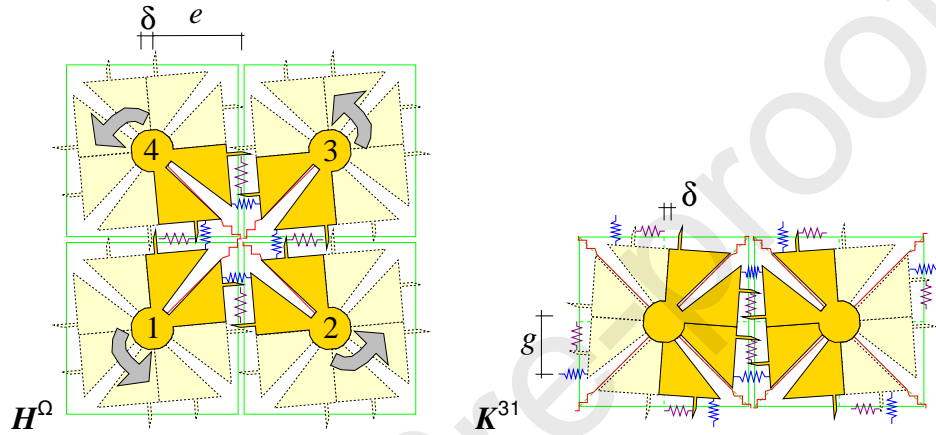


Figure 17: Deformed CSPF-molecule: Micro-rotation deformation condition (left). In-plane bending (right).

while the corresponding elastic energy density in the UC is:

$$\mathcal{U}_{\text{CSPF}}^\Omega = 2c^M \omega^2 \quad (45)$$

On the other hand, the deformation associated to the in-plane bending cannot be homogeneous and it implies a gradient of the axial strain, as shown in Figure 17, on the right side. In this case the size effect also plays a role and thus it is necessary to explicitly establish the size of the domain that is considered for the evaluation of the elastic parameters. In the present manuscript the calibration of the distance g is based on the unit cell shown on the right part of Figure 17 and thus only the deformation of the two axial \mathbf{B} -blue bond-springs, $\varepsilon_{K31}^B = \frac{g}{e} \omega$, is considered. The value attributed to the $\frac{g}{e}$ ratio determines the level of flexural coupling between the rigid elements, or atoms. Several choices can be made, however the preferable one is to place the axial springs in the Gauss points for the optimal integration of a linear distribution of stress along the connection side. A possible alternative is to place the axial springs simply in the midpoint of the half-side in common. To this basic choice, a management of scale effects can also be added, as proposed in Casolo (2004).

4.3.1. CSPF-relationship with a polar continuum

To relate the elastic properties of the CSPF molecule with an enriched continuum material, e.g. in the case of isotropic plane stress Cosserat solid, it is usefull to express the constitutive relation as follows:

$$\begin{Bmatrix} S_{11} \\ S_{22} \\ S_{12} \\ S_{21} \\ M_{31} \\ M_{32} \end{Bmatrix} = 2G \begin{bmatrix} \frac{1}{1-\nu} & \frac{\nu}{1-\nu} & 0 & 0 & 0 & 0 \\ \frac{\nu}{1-\nu} & \frac{1}{1-\nu} & 0 & 0 & 0 & 0 \\ 0 & 0 & \frac{1+\theta}{2} & \frac{1-\theta}{2} & 0 & 0 \\ 0 & 0 & \frac{1-\theta}{2} & \frac{1+\theta}{2} & 0 & 0 \\ 0 & 0 & 0 & 0 & d^2 & 0 \\ 0 & 0 & 0 & 0 & 0 & d^2 \end{bmatrix} \begin{Bmatrix} E_{11} \\ E_{22} \\ E_{12} \\ E_{21} \\ K_{31} \\ K_{32} \end{Bmatrix} \quad (46)$$

where the parameter $\theta = \kappa/G$ governs the specific skew symmetric contribute to the shear elastic response. In the case of a unit cell subjected to a pure micro-rotation $E_\omega = -\omega$, the elastic energy density of this continuum is $\mathcal{U}_{\text{Cosserat}}^\Omega = 2G\theta\omega^2$, and by comparing this value with Eq. 45 we find:

$$c^M = \theta G = \kappa \quad (47)$$

and thus the following relationship holds between the Poisson ratio ν and the parameter θ for this type of discrete model:

$$\theta = \frac{1-3\nu}{1-\nu} \quad (48)$$

for the plane stress case. This relationship between the Poisson's ratio and the parameter θ implies that $C_{12} = C_{34}$. It is also worth noting that the singular case of $\nu = 0 \rightarrow \theta = 1$ and corresponds to a CSPF molecule lacking the *R*-red diagonal bond-spring and a Cosserat material with only the diagonal shear moduli $C_{33} = C_{44} = G$. The other singular case is for $\nu = \frac{1}{3} \rightarrow \theta = 0$, for which the CSPF molecule lacks the *M*-magenta shear bond-spring, and can be related to a simple Cauchy continuum with $C_{12} = C_{21} = C_{33} = C_{34} = C_{43} = C_{44} = G$, like Eqs. (31). Clearly, similar considerations hold for the case of plane strain.

The flexural stiffness $2Gd^2$ in Eq.(46) depends on the length d that can be evaluated by comparing the elastic energy stored in the UC represented on the right side of Figure 17, with the corresponding energy stored in a Cosserat solid continuum cell subjected to an in-plane curvature $K_{31} = \frac{\omega}{e} = \frac{\delta}{e^2}$.

$$\mathcal{U}_{\text{RBSM}}^K = c^B \left(\frac{g}{e} \right)^2 \omega^2 = Gd^2 K_{31}^2 = \mathcal{U}_{\text{Cosserat}}^K \quad (49)$$

which implies that $d = g$, being $c^B = G$. This result also offers a practical interpretation to the geometrical parameter d , which is simply equal to the arm of the axial bond-springs, that governs the micro-polar in-plane stiffness.

4.4. Elasticity of the Cosserat-molecule

The scheme of this UC is obtained by adding a *G*-green shear bond-spring connection along each of the two diagonals, and consequently two more strain

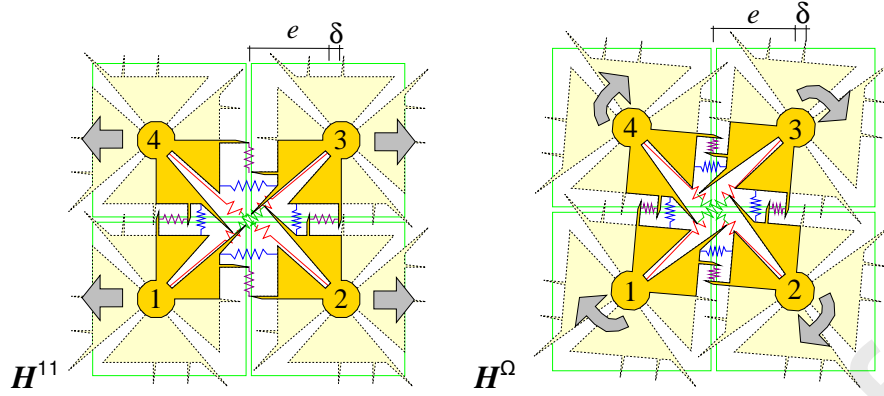


Figure 18: Deformed Cosserat-molecule: Uniaxial (left) and micro-rotation (right).

measures γ_{13}^G and γ_{24}^G are required. The measures of strain associated to this UC are assembled in the following vector of 12 components:

$$\{\mathcal{E}_{\text{Cosserat}}\}^T = \{\mathcal{E}_{13}^R, \mathcal{E}_{24}^R, \mathcal{E}_{12}^B, \mathcal{E}_{23}^B, \mathcal{E}_{34}^B, \mathcal{E}_{41}^B, \gamma_{13}^G, \gamma_{24}^G, \gamma_{12}^M, \gamma_{23}^M, \gamma_{34}^M, \gamma_{41}^M\} \quad (50)$$

The elastic moduli of the corresponding bond-springs are assembled in

$$\{\text{diag}[C]\}^T = \{c^R, c^R, c^B, c^B, c^B, c^B, c^G, c^G, c^M, c^M, c^M, c^M\} \quad (51)$$

To evaluate the elastic moduli of the four types of bond-spring, the 4 homogeneous displacement gradient fields, already described in the previous subsections, are used. The hydrostatic \mathbf{H}^H and the deviatoric \mathbf{H}^D do not cause any strain to the new G -green bond-springs, while the uniaxial \mathbf{H}^{11} and the micro-rotation \mathbf{H}^Ω displacement fields imply a strain in the G -green bond-springs, as shown in the Fig. 18. According to the linear relation for the strains given by Eq.(19), then the vectors with the measures assigned to the corresponding springs are:

$$\begin{aligned} \{\mathcal{E}^H\}^T &= \{\epsilon, \epsilon, \epsilon, \epsilon, \epsilon, \epsilon, 0, 0, 0, 0, 0, 0\} \\ \{\mathcal{E}^D\}^T &= \{\epsilon, -\epsilon, 0, 0, 0, 0, 0, 0, -\epsilon, \epsilon, -\epsilon, \epsilon\} \\ \{\mathcal{E}^{11}\}^T &= \{\epsilon/2, \epsilon/2, \epsilon, 0, \epsilon, 0, -\epsilon/2, \epsilon/2, 0, 0, 0, 0\} \\ \{\mathcal{E}^\Omega\}^T &= \{0, 0, 0, 0, 0, 0, \epsilon, \epsilon, -\epsilon, -\epsilon, -\epsilon, -\epsilon\} \end{aligned} \quad (52)$$

while the elastic energy densities in a unit cell, are:

$$\begin{aligned} \mathcal{U}_{\text{RBSM}}^H &= (c^R + 2c^B) \epsilon^2 \\ \mathcal{U}_{\text{RBSM}}^D &= (c^R + 2c^M) \epsilon^2 \\ \mathcal{U}_{\text{RBSM}}^{11} &= (\frac{1}{4}c^R + c^B + \frac{1}{4}c^G) \epsilon^2 \\ \mathcal{U}_{\text{RBSM}}^\Omega &= (c^G + 2c^M) \epsilon^2 \end{aligned} \quad (53)$$

4.4.1. Cosserat-molecule relationship with a Cosserat continuum

The corresponding elastic energy densities in a plane stress Cosserat are:

$$\begin{aligned}
 \mathcal{U}_{\text{Cosserat}}^{\text{H}} &= 2 \frac{1+\nu}{1-\nu} G \epsilon^2 \\
 \mathcal{U}_{\text{Cosserat}}^{\text{D}} &= 2G \epsilon^2 \\
 \mathcal{U}_{\text{Cosserat}}^{11} &= \frac{1}{1-\nu} G \epsilon^2 \\
 \mathcal{U}_{\text{Cosserat}}^{\Omega} &= 2G\theta \epsilon^2
 \end{aligned} \tag{54}$$

By imposing equality, one to one, to Eqs.(54) with (53), it is found also in this case that $C_{12} = C_{34}$ together with the relation between θ and ν given by Eq.(48). The system of equations is indeterminate, the rank is 3, and thus it is possible to assign a value to the B -blue bond-spring c^B and express the other three moduli as a function of it, as follows:

$$\begin{aligned}
 c^R &= 2G \frac{1+\nu}{1-\nu} - 2c^B \\
 c^M &= -2G \frac{\nu}{1-\nu} + c^B \\
 c^G &= 2G - 2c^B
 \end{aligned} \tag{55}$$

When assuming $c^B = G$ we return to the previous case where $c^G = 0$, i.e. without the G -green bond-spring.

The main interest here is to investigate the case of $c^B \in (0, G]$, because in this range it is possible to obtain a UC with auxetic isotropic response with Poisson coefficient $\nu \in (-1, 0]$, and with the springs moduli that remain in the positive field. Two examples are reported in Figure 19, which shows the trends of the springs moduli when assuming $c^B = G/2$ and $c^B = G/10$.

A first noticeable situation occurs in the case $\nu = 0$ which corresponds to equal values of the couples of red-green moduli ($c^R = c^G$) and blue-magenta moduli ($c^B = c^M$). Overall, it is noted that by reducing the modulus of c^B then it is possible to obtain lower negative Poisson ratio values, until ν becomes close to -1 when c^B is very small, and in this case also the R -red bond-spring is correspondingly very small. Thence, in this limit case the corresponding heuristic molecule is “almost” without the axial springs, as shown in the heuristic representation of Figure 20. It worth to note that the behaviour and also the topology of this UC, resamble the periodic structure of the radially keyed graphite brick moderator core of a Magnox nuclear reactor (Davies, 1995). That structure was required to have a high stiffness to shear deformation in the horizontal plane and a low resistance to volume change (Evans and Alderson, 2000). At the macro-scale, the micro-structured material expands isotropically in all radial directions when subjected to a tensile load and is auxetic with ν close to -1 in the horizontal plane.

A numerical investigation about the effective isotropy of the proposed Cosserat heuristic molecule has been performed by following the same approach described in section 4.2.1. The Figure 21 shows a graphical synthesis

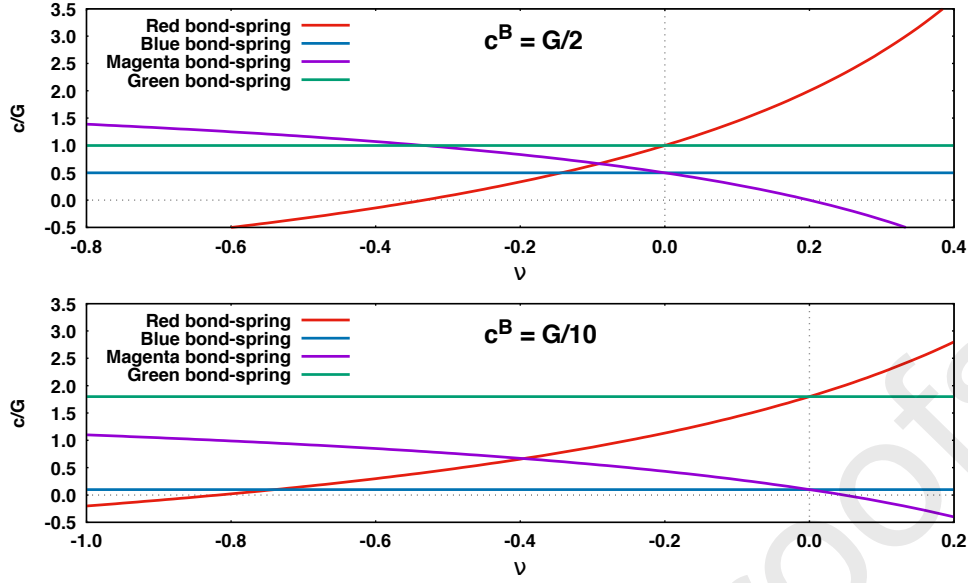


Figure 19: Variation of the bond-spring moduli with ν for $c^B = G/2$ and $c^B = G/10$.

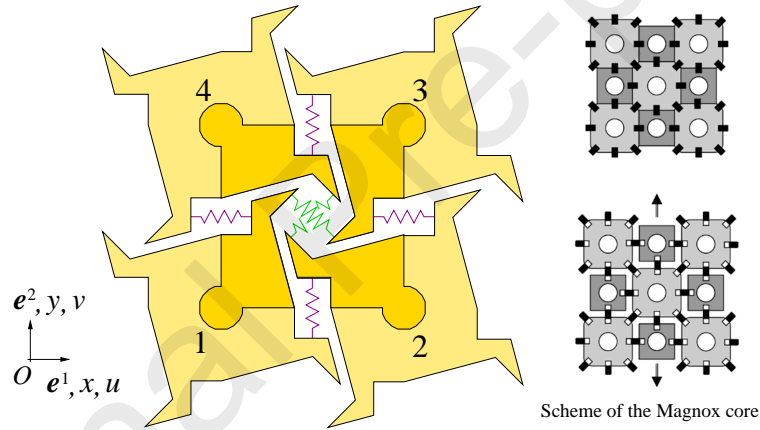


Figure 20: Sketch of a UC of Cosserat type with an auxetic microstructure which gives a Poisson ratio very close to -1 . In this representation the axial (blue and red) springs are not drawn because of the small values of their elastic moduli in comparison with the shear springs (magenta and green).

of the elastic response of this UC arrangement by plotting the ratio of the strain energy stored in the UC, $\frac{\mathcal{U}(\theta)}{\mathcal{U}(0)}$, when subjected to a given deformation which is rotated at angle θ with respect to the initial reference system.

260 The two drawings in the first row show the responses in the case of $c^B = G/2$, and the different curves refer to values of the Poisson ratio in the range $(-\frac{1}{3}, \frac{1}{5})$, which allows to obtain positive values for all the elastic moduli of the bond-springs. The two drawings in the second row show the responses in the case of $c^B = G/10$, which allows to consider values of the Poisson ratio in the range

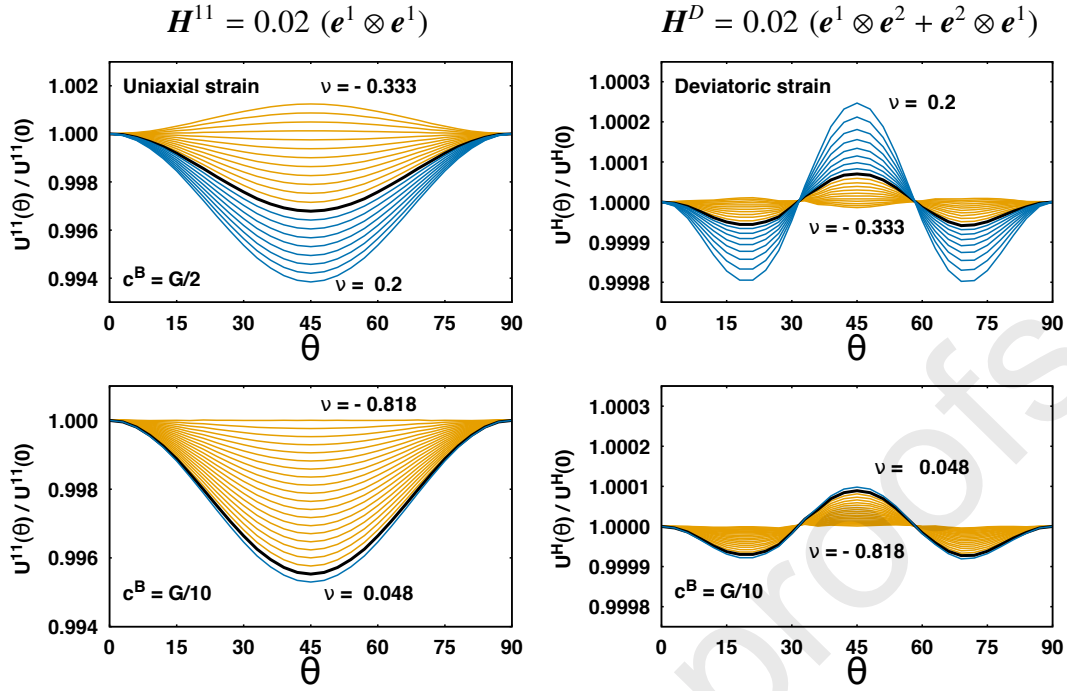


Figure 21: Plot of the ratio $\frac{\mathcal{U}(\theta)}{\mathcal{U}(0^\circ)}$ (elastic energy evaluated for a deformation field applied at different orientation θ , over the elastic energy corresponding to the deformation at $\theta = 0^\circ$). Left: uniaxial tensile deformation; Right: pure deviatoric deformation. Orange lines refer to negative Poisson ratios, blue lines refer to positive Poisson ratios, while the thick black line refers to $\nu = 0$.

265 $(-\frac{9}{11}, \frac{1}{21})$, giving positive values to all the elastic moduli of the bond-springs.

These results shows that the model is able give a very good approximation of the isotropy, and this happens even for a value of the Poisson ratio that becomes close to the limit value of -1 .

5. Some concluding remarks

270 The present study has been developed according to the idea of modelling the macroscale elastic response of a solid material, which can be homogeneous as well as a regular composite, by means a full discrete approach. The core consists in the design of a “heuristic molecule” that is the minimum unit cell, UC, that contains all the macroscopic mechanical properties of the solid material object of interest. This UC is an assemblage of rigid bodies that can have a
 275 definite shape, bonded by elastic springs. The concept of material point, typical of the continuum approach, cannot be applied here, and thus the constitutive laws that describe the macroscale properties involve the relative displacements of its rigid bodies, or heuristic atoms. Despite this, the approach substantially
 280 respects the priciple of local action if we accept that the UC delimits a corresponding domain of the local action, and it is the smallest limit below which the solid material model cannot be described.

The approach of identifying “simple machines” within materials is somehow in accordance with a mechanistic spirit that can be traced back to Leonardo da Vinci and Galileo Galilei, and allows to rediscover a physical-inductive aspect in solid mechanics modelling that sometimes tends to remain hidden behind the purely mathematical-deductive formulations. To support this, it is worth quoting Galilei (1638): “tutte le ragioni della mecanica hanno i fondamenti loro nella geometria”[sic].⁷

The paper has been developed by designing and analyzing the topology of 4 unit cells in progression from the most basic (CF-molecule) to the most refined (Cosserat-molecule). Particular emphasis has been given to the requirement of an isotropic response in relation to the value of the macroscopic Poisson ratio. In fact, it is well known that this aspects constituted an initial shortcoming for the success of a solid mechanics modelled on a discrete basis rather than on a continuum approach (Capecchi et al., 2010). A square cell consisting of 4 rigid elements has been adopted for the different UCs, and the rigid bodies (which in the CF case were simple “material points ” connected by central springs) have been gradually enhanced by giving them a shape and size. The evaluation of the performance in terms of isotropy was done numerically, on a single UC, so as to be able to also take into account the effects of the approximations in the deformation measurements attributed to the springs, considering the variation of the elastic energy as a function of the orientation angle for displacements that corresponded to a uniaxial extension and to a purely deviatoric deformation field. In this way, it has been shown how the elastic connections should include the shear actions in order to widen the range of the isotropic response to Poisson ratio values until approaching the limit of -1 .

The potential interest, from the point of view of engineering materials with periodic internal structure is oriented at designing materials with non-standard mechanical properties: polar, chiral and auxetic (Spadoni and Ruzzene, 2012; Liu et al., 2012; Dos Reis and Ganghoffer, 2012; Lakes, 2017; Bacigalupo and Gambarotta, 2020; Auricchio et al., 2019; Gao et al., 2020; Ieşan, 2020; Ruschel and Zok, 2020). In this sense, the example of the topology of the moderator core of a Magnox nuclear reactor has been shown, demonstrating that is substantially consistent with what derives from the proposed Cosserat heuristic molecule when the Poisson’s ratio tends to the limit of -1 . Another aspect of the design potentiality of this approach has been observed in the CFSP molecule where the arm separating the blue axial springs can be directly correlated to the characteristic length of a Cosserat continuum.

On the other hand, the approach is also suitable for a direct implementation for numerical applications, for example by finite elements, since the

⁷[translation:] “all the explanations of mechanics have fundaments in their geometry”, sentence pronounced by Sagredi in the Discourses and Mathematical Demonstrations Around Two New Sciences, at the beginning of the first day Galilei (1638).

stiffness matrix of the master finite element can be directly obtained from the heuristic molecule. In theory, the informations about the topology aspects of the constitutive behaviour of the material can be introduced by means of a matrix $[L]$, as introduced in section 2. In practice, under the hypothesis of small displacements and adopting a linearized kinematics, this can be obtained by directly assembling a matrix $[B]$ that relates the displacement of the rigid bodies with the strains of the bond-springs, as shown in Eq. (19). As a result, the pure elastic relation assumed for the springs remains described by a diagonal operator. In this perspective the concept of stress tensor is no more needed, and also the passage through differential operators can be avoided (Tonti, 2014). Table 1 schematically resumes a comparison between the heuristic and the continuum approach, showing that the main difference is the transfer of information about the internal topology of the material to the macro-scale, by the process of assemblage of operator $[B]$.

Table 1: Heuristic-molecule vs. solid continuum: Schematic comparison.

heuristic-molecule		solid continuum
$[X]$	position	\mathbf{x}
$[U]$	displacement	\mathbf{u}
$[L]$	local geometry	-
$\{\varepsilon\} = [B]\{u\}$	strain	$\mathbf{E} = \text{sym}\nabla\mathbf{u}$
$\mathcal{U} = \frac{1}{2}\{\varepsilon\}^T [\text{Diag}\{c\}]\{\varepsilon\}$	elasticity	$\mathcal{U} = \frac{1}{2}\mathbf{E} \cdot \mathbb{C}\mathbf{E}$
$[K]\{u\} = \{p\}$	solid element	$[K]\{u\} = \{p\}$
\searrow algebraic numerical solution		\swarrow

References

- Auricchio, F., Bacigalupo, A., Gambarotta, L., Lepidi, M., Morganti, S., Vadalà, F., 2019. A novel layered topology of auxetic materials based on the tetrachiral honeycomb microstructure. *Materials & Design* 179, 107883. doi:https://doi.org/10.1016/j.matdes.2019.107883.
- Bacigalupo, A., Gambarotta, L., 2020. Chiral two-dimensional periodic blocky materials with elastic interfaces: Auxetic and acoustic properties. *Extreme Mechanics Letters* 39, 100769. doi:https://doi.org/10.1016/j.eml.2020.100769.
- Ballarini, R., Diana, V., Biolzi, L., Casolo, S., 2018. Bond-based peridynamic modelling of singular and nonsingular crack-tip fields. *Meccanica* 53, 3495–3515. doi:10.1007/s11012-018-0890-7.
- Benvenuto, E., 1991. An introduction to the history of structural mechanics. Springer-Verlag, New York.

- Birck, G., Iturrioz, I., Lacidogna, G., Carpinteri, A., 2016. Damage process in heterogeneous materials analyzed by a lattice model simulation. *Engineering Failure Analysis* 70, 157 – 176. doi:10.1016/j.engfailanal.2016.08.004.
- Bolander, J., Saito, S., 1998. Fracture analyses using spring networks with random geometry. *Engineering Fracture Mechanics* 61, 569 – 591. doi:10.1016/S0013-7944(98)00069-1.
- Brighenti, R., Carpinteri, A., Spagnoli, A., Scorza, D., 2013. Cracking behaviour of fibre-reinforced cementitious composites: A comparison between a continuous and a discrete computational approach. *Engineering Fracture Mechanics* 103, 103 – 114. doi:10.1016/j.engfracmech.2012.01.014.
- Capecchi, D., Ruta, G., Trovalusci, P., 2010. From classical to Voigt's molecular models in elasticity. *Archive for History of Exact Sciences* 64, 525–559. doi:10.1007/s00407-010-0065-y.
- Casolo, S., 2004. Modelling in-plane micro-structure of masonry walls by rigid elements. *International Journal of Solids and Structures* 41, 3625–3641. doi:10.1016/j.ijsolstr.2004.02.002.
- Casolo, S., 2006. Macroscopic modelling of structured materials: Relationship between orthotropic Cosserat continuum and rigid elements. *International Journal of Solids and Structures* 43, 475 – 496. doi:10.1016/j.ijsolstr.2005.03.037.
- Casolo, S., 2009. Macroscale modelling of microstructure damage evolution by a rigid body and spring model. *Journal of Mechanics of Materials and Structures* 4, 551–570. doi:10.2140/jomms.2009.4.551.
- Cusatis, G., Pelessone, D., Mencarelli, A., 2011. Lattice discrete particle model (LDPM) for failure behavior of concrete. i: Theory. *Cement and Concrete Composites* 33, 881 – 890. doi:10.1016/j.cemconcomp.2011.02.011.
- Davies, M., 1995. Graphite core design in UK reactors., in: Specialists meeting on graphite moderator lifecycle behaviour, International Atomic Energy Agency, Vienna(Austria). IAEA-TECDOC-901, Bath, UK. p. 47–56.
- Dell'Isola, F., Giorgio, I., Pawlikowski, M., Rizzi, N., 2016. Large deformations of planar extensible beams and pantographic lattices: Heuristic homogenization, experimental and numerical examples of equilibrium. *Proceedings of the Royal Society A: Mathematical, Physical and Engineering Sciences* 472. doi:10.1098/rspa.2015.0790.
- Diana, V., Carvelli, V., 2020. An electromechanical micropolar peridynamic model. *Computer Methods in Applied Mechanics and Engineering* 365. doi:10.1016/j.cma.2020.112998.

- Diana, V., Casolo, S., 2019. A bond-based micropolar peridynamic model with shear deformability: Elasticity, failure properties and initial yield domains. *International Journal of Solids and Structures* 160, 201 – 231. doi:https://doi.org/10.1016/j.ijsolstr.2018.10.026.
- Dos Reis, F., Ganghoffer, J., 2012. Equivalent mechanical properties of auxetic lattices from discrete homogenization. *Computational Materials Science* 51, 314 – 321. doi:https://doi.org/10.1016/j.commatsci.2011.07.014.
- Eremeyev, V., Turco, E., 2020. Enriched buckling for beam-lattice metamaterials. *Mechanics Research Communications* 103. doi:10.1016/j.mechrescom.2019.103458.
- Evans, K.E., Alderson, A., 2000. Auxetic materials: Functional materials and structures from lateral thinking! *Advanced Materials* 12, 617–628. doi:10.1002/(SICI)1521-4095(200005)12:9<617::AID-ADMA617>3.0.CO;2-3.
- Ferretti, E., 2013. The cell method: An enriched description of physics starting from the algebraic formulation. *Computers, Materials and Continua* 36, 49–71.
- Foce, F., 1995. Between Mechanics and Architecture (E. Benvenuto and P. Radelet-de Grave, eds.). Birkhäuser, Basel. chapter The theory of elasticity between molecular and continuum approach in the XIXth century. pp. 301–314.
- Galilei, G., 1638. *Discorsi e dimostrazioni matematiche, intorno à due nuove scienze*. Appresso gli Elsevirii, Leida.
- Gao, Y., Wu, Q., Wei, X., Zhou, Z., Xiong, J., 2020. Composite tree-like re-entrant structure with high stiffness and controllable elastic anisotropy. *International Journal of Solids and Structures* 206, 170–182. doi:10.1016/j.ijsolstr.2020.09.003.
- Gerstle, W., Sau, N., Silling, S., 2007. Peridynamic modeling of concrete structures. *Nuclear Engineering and Design* 237, 1250 – 1258. doi:10.1016/j.nucengdes.2006.10.002. 18th International Conference on Structural Mechanics in Nuclear Engineering.
- Griffiths, D.V., Mustoe, G.G.W., 2001. Modelling of elastic continua using a grillage of structural elements based on discrete element concepts. *International Journal for Numerical Methods in Engineering* 50, 1759–1775. doi:10.1002/nme.99.
- Ieşan, D., 2020. Generalized plane strain of chiral elastic solids. *Mechanics Research Communications* 107. doi:10.1016/j.mechrescom.2020.103564.

- 425 Jiang, C., Zhao, G.F., Khalili, N., 2017. On crack propagation in brittle material using the distinct lattice spring model. *International Journal of Solids and Structures* 118-119, 41 – 57. doi:<https://doi.org/10.1016/j.ijsolstr.2017.04.024>.
- Lakes, R., 2017. Negative-poisson's-ratio materials: Auxetic solids. *Annual Review of Materials Research* 47, 63–81. doi:10.1146/annurev-matsci-070616-124118.
- 430 Liu, X., Huang, G., Hu, G., 2012. Chiral effect in plane isotropic micropolar elasticity and its application to chiral lattices. *Journal of the Mechanics and Physics of Solids* 60, 1907 – 1921. doi:<https://doi.org/10.1016/j.jmps.2012.06.008>.
- 435 Love, A., 1926. *A treatise on the mathematical theory of elasticity*. 4 ed., Dover, New York.
- Maxwell, J., 1853. On the equilibrium of elastic solids. *Trans. of the Royal Society of Edinburgh* 20, 87–120.
- Ostoj-Starzewski, M., 2002. Lattice models in micromechanics. *Applied Mechanics Reviews* 55, 35–59. doi:10.1115/1.1432990.
- 440 Poisson, S.D., 1831. Mémoire sur les équations générales de l'équilibre et le du mouvement des corps solides élastiques et des fluides. *Journal de l'École polytechnique* 13, 1–174.
- Rossetti, D., 1671. *Composizione e passione de'vetri*. Ed. G V Bonfigli, Livorno.
- 445 Ruschel, A.L., Zok, F.W., 2020. A bi-material concept for periodic dissipative lattices. *Journal of the Mechanics and Physics of Solids* 145, 104144. doi:<https://doi.org/10.1016/j.jmps.2020.104144>.
- Spadoni, A., Ruzzene, M., 2012. Elasto-static micropolar behavior of a chiral auxetic lattice. *Journal of the Mechanics and Physics of Solids* 60, 156 – 171. doi:<https://doi.org/10.1016/j.jmps.2011.09.012>.
- 450 Stakgold, I., 1950. The Cauchy relations in a molecular theory of elasticity. *Quarterly of Applied Mathematics* 8, 169–186. doi:10.1090/qam/36650.
- Tonti, E., 2001. A direct discrete formulation of field laws: The cell method. *CMES - Computer Modeling in Engineering and Sciences* 2, 237–258.
- 455 Tonti, E., 2014. Why starting from differential equations for computational physics? *Journal of Computational Physics* 257, 1260 – 1290. doi:<https://doi.org/10.1016/j.jcp.2013.08.016>. physics-compatible numerical methods.

- 460 Turco, E., Dell'Isola, F., Cazzani, A., Rizzi, N., 2016. Hencky-type discrete model for pantographic structures: numerical comparison with second gradient continuum models. *Zeitschrift für Angewandte Mathematik und Physik* 67, 1–28. doi:10.1007/s00033-016-0681-8.
- Vannucci, P., Desmorat, B., 2016. Plane anisotropic rari-constant materials. *Mathematical Methods in the Applied Sciences* 39, 3271–3281. doi:10.1002/mma.3770.
465
- Voigt, W., 1887. Theoretische Studien über die Elasticitätsverhältnisse der Kristalle. *Abhandlungen der Gesellschaft der Wissenschaften Zu Göttingen—Mathematische Classe* 34(3), 3–100.
- 470 Voigt, W., 1900. L'état actuel de nos connaissances sur l'élasticité des cristaux, in: Guillaume, C.E., Poincaré, L. (Eds.), *Rapports présentés au Congrès international de Physique*, Gautier-Villars, Paris. pp. 277–347.
- Wang, Y., Mora, P., 2008. Macroscopic elastic properties of regular lattices. *Journal of the Mechanics and Physics of Solids* 56, 3459 – 3474. doi:https://doi.org/10.1016/j.jmps.2008.08.011.
- 475 Yao, C., Jiang, Q., Shao, J., Zhou, C., 2016. A discrete approach for modeling damage and failure in anisotropic cohesive brittle materials. *Engineering Fracture Mechanics* 155, 102 – 118. doi:10.1016/j.engfracmech.2016.01.012.
- 480 Zhao, S.F., Zhao, G.F., 2012. Implementation of a high order lattice spring model for elasticity. *International Journal of Solids and Structures* 49, 2568 – 2581. doi:https://doi.org/10.1016/j.ijsolstr.2012.05.015.